Vibrational Spectroscopy as a Probe of Structure and Dynamics in Liquid Water

H. J. Bakker*,† and J. L. Skinner*,‡

FOM Institute for Atomic and Molecular Physics, Kruislaan 407, 1098 SJ Amsterdam, The Netherlands, and Theoretical Chemistry Institute and Department of Chemistry, University of Wisconsin, Madison, Wisconsin 53706

Received May 10, 2009

Contents

1. Introduction

Water is, of course, a fascinating and important substance. For such a simple molecule, its condensed phase properties are surprisingly complex. Here we might mention the many different solid phases, the higher density of the liquid as compared to ice I_h, and the density maximum (as a function of temperature) in the liquid phase. Moreover, for such a light molecule, many of the liquid-state properties are anomalous: the boiling point, freezing point, heat capacity, surface tension, and viscosity are all unusually high. Even so, it is perhaps surprising that we still do not fully understand the properties of the liquid state.[1−3]

From a theoretical point of view, this can probably be attributed to two features of liquid water: cooperative hydrogen bonding (H-bonding) and nuclear quantum effects. The former refers to the fact that the binding energy of two H-bonded molecules is modified by the presence of a third molecule.[4−9] In terms of simulating the liquid, then, it follows that the potential energy cannot be written as a sum of two-molecule terms. This means that simple two-body simulation models cannot completely describe reality, and attempts to capture the effects of these many-body interactions with polarizable models are not fully satisfactory either.[8,10] Nuclear quantum effects occur because the hydrogen nucleus is sufficiently light that classical mechanics for the nuclear motion is simply not adequate. Thus, classical mechanics cannot describe such important properties as spatial dispersion of the hydrogen positions, nuclear tunneling, zero-point energy, and quantization of nuclear motions. Much energy has recently been expended toward the simulation of liquid water using *ab initio* electronic-structure methods (which, in priniciple, will produce the correct Born−Oppenheimer potential surface, including the effects of many-body interactions),[11−19] together with methods for quantum dynamics,[19−25] but still more work needs to be done before we have a complete and accurate description.

On the experimental side, one is limited by the existing experimental techniques that have been brought to bear on the problem—these techniques include nuclear magnetic resonance (NMR);[26−31] dielectric relaxation;[32] X-ray scattering;[33] X-ray absorption, emission, and Raman spectroscopies;[34,35] elastic and inelastic neutron scattering;[36−38] and THz spectroscopy.[39,40] For example, NMR is very useful for measuring the correlation times for rotation of various molecule-fixed axes, but it cannot provide the time dependence of the rotational correlation functions. X-ray scattering is primarily sensitive to oxygen positions and can provide the oxygen−oxygen radial distribution function but cannot say much about higher-order oxygen-position correlations or about hydrogen positions. Through the use of isotope-substitution experiments,[36] neutron scattering does provide information about both hydrogen and oxygen positions but, again, not about higher-order correlations. The new techniques of X-ray absorption, emission, and Raman scattering are sensitive to the electronic excited states of the liquid, which are difficult to calculate, perhaps explaining why interpretation of these experiments has not been unambiguous.[34,35,41]

In this review, we discuss the experimental technique of vibrational spectroscopy and the role that it has played in elucidating the structure and dynamics of liquid water in thermal equilibrium. These techniques begin with the straight-

* To whom correspondence should be addressed.
† FOM Institute for Atomic and Molecular Physics.
‡ University of Wisconsin, Madison.

10.1021/cr9001879
Published on Web 11/16/2009

Huib Johan Bakker was born on March 2, 1965, in Haarlem, The Netherlands. He did his Ph.D. studies in the group of Prof. dr. Ad Lagendijk, at the FOM Institute for Atomic and Molecular Physics (AMOLF). From 1991 to 1994 he worked as a postdoc in the group of Prof. dr. Heinz Kurz at the Institute of Semiconductor Electronics at the Technical University of Aachen, Germany. In 1995 he became a group leader at AMOLF, heading the group "Ultrafast Spectroscopy". The research work of the group includes the spectroscopic study of the structure and ultrafast dynamics of water interacting with ions and (bio)molecular systems and the study of the mechanism of proton transfer in aqueous media. In 2001 he became a full professor of Physical Chemistry at the University of Amsterdam, The Netherlands. In 2004, he received the Gold Medal of the Royal Netherlands Chemical Society for his work on the ultrafast dynamics of aqueous systems.

James Lauriston Skinner received his Ph.D. from Harvard under the direction of Prof. Peter Wolynes in 1979, and he did postdoctoral work with Hans Andersen at Stanford. He then spent nine years on the faculty of Columbia University, becoming full professor in 1986. In 1990 he moved to the University of Wisconsin as the Joseph O. Hirschfelder Professor of Chemistry and Director of the Theoretical Chemistry Institute, positions he currently occupies. His research interests involve the structure, dynamics, relaxation, and spectroscopy of condensed-phase systems.

forward infrared (IR) absorption experiments of many years ago, followed by polarized and depolarized Raman scattering experiments within the last 40 years and ultrafast IR and Raman experiments of the past decade.[42−45] Vibrational spectroscopy is a useful technique for studying the structure and dynamics of water for two reasons. First, vibrational frequencies, especially in the OH stretch region, are very sensitive to molecular environment, including H-bonding. Thus, a simple absorption experiment, which in large part measures the ensemble of vibrational frequencies in the liquid, reflects the distributions of local environments, which, in turn, is intimately related to the structure of the liquid. Local structure, of course, evolves in time due to molecular dynamics. As such, the frequency of any one OH stretch also fluctuates in time—a process known as spectral diffusion. A time-resolved experiment with laser-pulse durations on the time scale of molecular motion in the liquid, or shorter, in principle can measure the statistics of spectral diffusion, which, in turn, provides an excellent probe of molecular dynamics. The second fundamental reason that vibrational spectroscopy is so useful is that the transition dipole vector and polarizability tensor of a molecule, relevant for IR and Raman spectroscopy, respectively, are tied to its molecule-fixed frame. Thus, for example, ultrafast IR spectroscopy with polarized lasers can provide a detailed probe of the dynamics of molecular rotation.[43]

For an isolated gas-phase water molecule, the two local-mode OH stretches are coupled, which leads to a splitting between the symmetric and antisymmetric stretch normal-mode frequencies of some 100 cm^{-1}. In condensed phases, the degeneracy of the two local-mode frequencies is broken, very strongly (in comparison with the coupling), due to different local environments, diminishing the effect of the coupling.[46] On the other hand, in condensed phases, there is also the possibility of vibrational coupling between OH stretches on different molecules. Our current understanding is that this coupling has a pronounced effect on instantaneous vibrational eigenstates for single excitations, which can extend over ten or more molecules.[47,48] Concomitantly, this delocalization has a pronounced effect on both the steady-state and ultrafast vibrational spectroscopy, causing, for example, the appearance of a collective vibrational peak in the polarized Raman spectrum[48] and the very rapid anisotropy decay (due to vibrational energy transfer) in pump−probe experiments.[49−54] In terms of the study of vibrational dynamics,[55−71] these are important and fascinating effects. They are, however, less relevant to the structure and dynamics of liquid water in thermal equilibrium (where all OH stretch vibrations are in their ground states).

Therefore, in order to study the structure and dynamics of liquid water in thermal equilibrium, it is more useful to employ isotopes, for example, by considering dilute HDO in D_2O or dilute HDO in H_2O (and, actually, Nicodemus and Tomakoff[72] have also looked at dilute HTO in H_2O). In these two situations, the OH or OD stretches, respectively, function as localized chromophores, since, because of substantial frequency mismatch, they are effectively uncoupled from all other stretches in the sample. This means that they can act as effective reporters of local structure and dynamics, unfettered by the complications of delocalization and energy transfer described above in neat H_2O. For these reasons, we will focus only on these two systems in this review.

Ultrafast vibrational spectroscopy has also been used to study vibrational energy relaxation in HDO:H_2O or HDO:D_2O, typically measuring the OD or OH stretch lifetime, respectively,[73−82] although some recent experiments have focused on bend lifetimes.[83,84] This process is fundamentally important for understanding water's role as a solvent for chemical and electron transfer reactions. However, knowledge of these rates provides only indirect information about the structure and dynamics of water in thermal equilibrium (and even this relies heavily on theoretical modeling). Therefore, except for the inescapable role vibrational relaxation plays in all vibrational spectroscopy, we will not focus on it herein.

Thus, the topic of this review is conventional and ultrafast vibrational spectroscopy—especially those techniques that shed light on H-bonding structure and dynamics, spectral

diffusion, and rotational dynamics—of dilute HDO in either liquid H_2O or D_2O, in the OD or OH stretch region, respectively. Earlier experiments focused on the latter, since it was easier to coax lasers to perform well at these shorter wavelengths, whereas with later developments it has become just as easy to perform experiments on the former. At this point, it might be worth mentioning that there is a slight preference for working on the HDO:H_2O system, for several different reasons. First, this system probes the structure and dynamics of H_2O (rather than D_2O), which is inherently more important. Second, the OD stretch lifetime is longer than the OH stretch lifetime, providing more dynamic range in the ultrafast experiments. Third, theoretical simulation models have been parametrized for H_2O (and usually not for D_2O), which makes modeling H_2O more reliable. On the other hand, in ultrafast experiments, one is often worried about local heating from vibrational relaxation, and these effects are more problematic for HDO:H_2O (since in this case the HDO concentration needs to be higher, as described below). Note, also, that nuclear quantum effects, not taken into account explicitly in classical simulations, are more important for H_2O than for D_2O. Interpretation of vibrational spectroscopic observables, especially for the most modern ultrafast techniques, is greatly facilitated by molecular dynamics simulations and associated theoretical spectroscopy. Thus, this review also focuses on these complementary computational efforts.

In the next section we discuss how conventional IR and Raman experiments, together with computer simulation and theoretical interpretation, shed some light on the problems of liquid structure and H-bonding. In section 3 we consider ultrafast experiments that can probe spectral diffusion, most commonly and conveniently characterized statistically by the frequency time-correlation function, and we discuss attempts to understand experimental results from computer simulation and theoretical modeling. In section 4 we consider pump−probe experiments that measure rotational anisotropy decay, discussing both short-time (inertial) and long-time (collective) dynamics, and comparing them with simulation and theory. In section 5 we conclude.

2. Vibrational Spectroscopy as a Probe of Structure

2.1. Experimental IR and Raman Line Shapes

IR and Raman (polarized, depolarized, and unpolarized) line shapes for dilute HDO in D_2O at room temperature are all rather similar and are characterized by a large red shift of roughly 300 cm^{-1} from the gas-phase OH stretch frequency (for HDO) of 3707 cm^{-1} and a breadth of between 250 and 300 cm^{-1}. Both the red shift and the spectral breadth are unusually large for a vibrational transition. The shift is generally believed to result from H-bonds to the H atom in HDO. Such H-bonds weaken and lengthen the covalent OH bond, leading to a red shift in the average frequency. Liquid water, being disordered, has a wide range of H-bond distances and angles, and, in addition, has some broken H-bonds. Since the OH stretch frequency is so sensitive to these H-bonds, the thinking is that the distribution of H-bond configurations leads to a distribution of OH stretch frequencies, which is reflected in the large spectral breadth. There are some subtle differences between the IR and Raman spectra, namely that the Raman line shape is shifted to the blue by about 30 cm^{-1}, and it also has a shoulder on the blue side that is absent in the IR spectrum.

The situation for HDO:H_2O is similar, although all (OD) frequencies are smaller (because of the heavier D atom). Thus, the gas-phase OD stretch frequency is 2724 cm^{-1}, the liquid-state red-shift is about 225 cm^{-1}, and the spectral breadths are between 160 and 180 cm^{-1}. Note that, as discussed below, the ratios of gas-phase frequencies and red shifts for the OD and OH stretches are roughly the same, while the ratio of the line widths is somewhat smaller. The slight blue shift and blue shoulder in the Raman spectra are also seen for this (HDO:H_2O) system.

From a theoretical perspective, the goal is to reproduce the line shapes as closely as possible and then use the simulation results and other theoretical analysis to address a number of questions. For example, are the general thoughts about the shift and broadening in these systems correct? Can we understand the differences between IR and Raman line shapes and between the HDO:D_2O and HDO:H_2O systems? What, if anything, are the line shapes telling us about H-bonding in liquid water? The idea has been pervasive in the literature, as evidenced by multiple Gaussian fits to line shapes[85,86] and the ability to burn narrow transient spectral holes,[87−90] that different H-bonding configurations correspond to relatively narrow frequency distributions, which together make up the observed spectra. Is this idea correct?

2.2. Theoretical Approaches to Vibrational Line Shapes

The modern starting point for the calculation of spectral line shapes comes from quantum time-correlation functions (TCFs).[91,92] Thus, in principle, one could simulate liquid water, treating all electrons and nuclei quantum mechanically, and use existing TCF expressions to obtain IR and Raman line shapes. For a variety of technical and computational reasons, we are not yet close to being able to proceed in this fashion. One approach is to treat the nuclear motion, which occurs either on an empirical[93−95] or *ab initio*[96] potential energy surface, classically. Notwithstanding issues having to do with the accuracy of either of these surfaces, especially for high-frequency (OH or OD stretch) motion, there is reason to be concerned with the adequacy of the classical approximation for high frequency (compared to $kT/\hbar$) and very anharmonic modes.[97] Therefore, a number of workers have instead considered a mixed quantum/classical approach, where (in the case, for example, of HDO:D_2O) the OH stretch is treated quantum mechanically, the water bends and OD stretches are neglected, and the other nuclear degrees of freedom are treated with classical mechanics. Even within this approach there are several critical issues to be addressed. First, one needs to define the potential surface for the classical degrees of freedom, which is typically taken to be an empirical surface for rigid water. And second, and perhaps more importantly, one needs to define the potential surface for the OH stretch motion. There are really two choices here: either one can use the empirical surface for rigid water,[98−109] together with a reference potential for the gas-phase stretch, or one can, independent of the empirical potential, use *ab initio* calculations to determine this surface.[110−112]

The efforts Skinner and co-workers have undertaken in recent years involve the mixed quantum/classical approach, using the SPC/E model[113] for a molecular dynamics (MD) simulation of rigid water and electronic structure (ES)

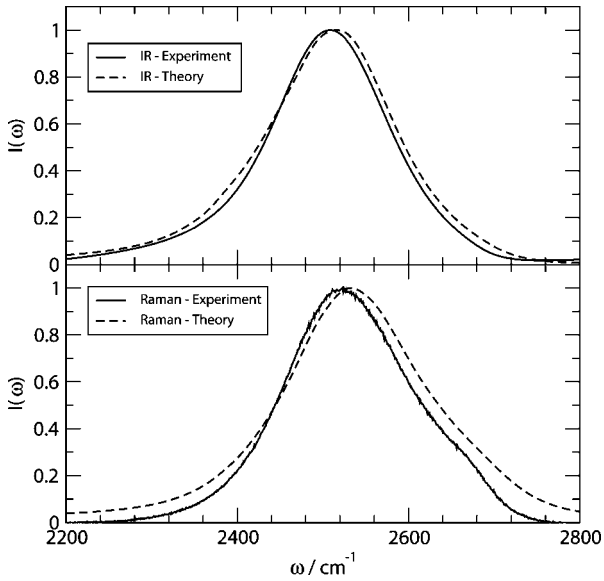

Figure 1. Theoretical[97] and experimental[124,125] IR and (unpolarized) Raman line shapes for dilute HDO in H_2O under ambient conditions. Reproduced with permission from ref 97. Copyright 2009 John Wiley and Sons.

calculations to determine the OH/OD stretch fundamental transition frequency for each simulation configuration.[97,112,114−118] In the latest implementation,[97,117,118] these ES calculations lead to a simple quadratic map between the vibrational frequency and the electric field, produced by the point charges of the surrounding molecules, at the H/D atom of interest, and in the direction of the OH/OD bond. With this map it is a simple matter to produce a frequency trajectory from the MD simulation. Another important spectral quantity is the transition dipole, which lies more or less along the OH/OD bond vector.[114,119] In liquid water the magnitude of this transition dipole depends strongly on the local environment,[120,121] which, in analogy with electronic spectroscopy, is called a non-Condon effect. It is important to take this non-Condon effect into account,[114,115] and so they developed an ES-based electric-field map for this quantity as well.[114,117] A similar (although much less important) non-Condon effect can be employed for the components of the transition polarizability tensor, which they implemented within the bond-polarizability model.[97,114,117] Armed with frequency, transition dipole, and transition polarizability trajectories, one can, within the mixed quantum/classical formulation, calculate IR and Raman spectra.[122] The results include the effects of motional narrowing,[123] and the broadening effects of molecular rotation, and vibrational relaxation (which is described phenomenologically).

In Figure 1 we show experimental[124,125] and theoretical[97] IR and (unpolarized) Raman line shapes for dilute HDO in H_2O at 298 K. There are no adjustable parameters in the theoretical calculation, except a scale factor that matches experimental and theoretical peak heights. In both cases, one sees quite reasonable agreement between experiment and theory. The slight blue shift of the Raman spectrum (with respect to the IR spectrum) and the weak shoulder on the blue side of the Raman spectrum are both captured by theory.

We can begin to answer some of the questions posed above, by considering the theoretical distribution of frequencies sampled by the ensemble of OD chromophores, the weighted (by the square of the transition dipole) frequency distribution (or spectral density) appropriate for the IR spectrum,[126] and the IR line shape, as shown in Figure 2.

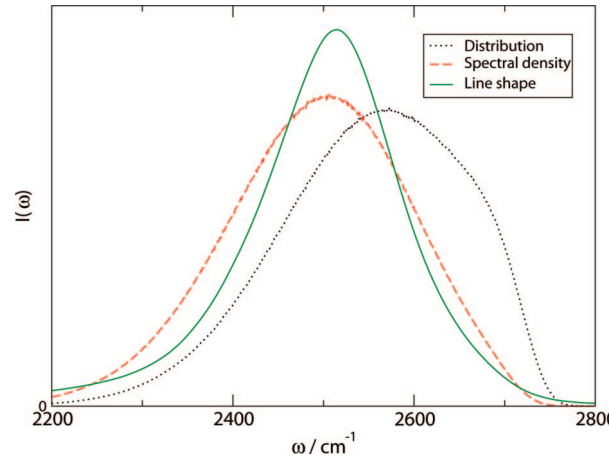

Figure 2. Theoretical frequency distribution, IR spectral density, and IR line shape, for dilute HDO in H_2O.

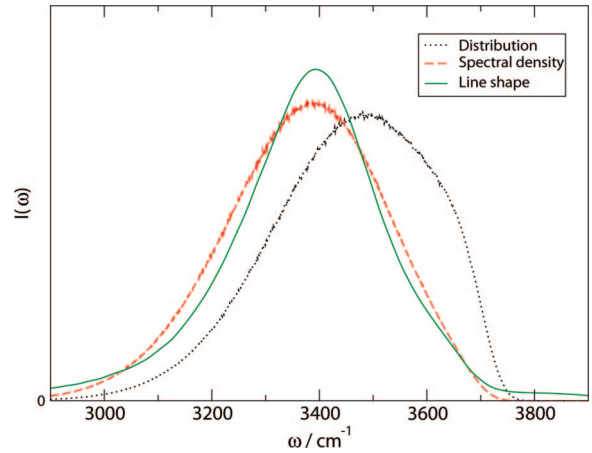

Figure 3. Theoretical frequency distribution, IR spectral density, and IR line shape for dilute HDO in D_2O.

All three curves have the same (area) normalization. The frequency distribution itself is quite asymmetrical, while the spectral density is more symmetrical and red-shifted. These differences are both due to non-Condon effects, since the transition dipole is much larger for molecules on the red side of the line.[114,115,117,127] Since non-Condon effects are much smaller for Raman spectroscopy, this immediately explains why the Raman spectrum is blue-shifted relative to the IR and why the shoulder (on the blue side) in the Raman spectrum is suppressed in the IR. The IR line shape is narrower than the spectral density due to motional narrowing (despite the weak broadening effects of rotations and vibrational relaxation). Still, the effects of motional narrowing are not dominant, and so the qualitative picture that the breadth of the line is determined by the distribution of frequencies is correct. In addition, the overall red shift clearly comes from H-bonding interactions with other molecules, as discussed above and as borne out by the ES calculations.

In Figure 3 we show the same quantities for HDO:D_2O, with similar conclusions, although in this case the amount of motional narrowing (relative to the spectral density) is smaller. This is easy to understand within the context of the simple Kubo model.[123] In this model the frequency fluctuations describe a Gaussian process and, hence, are characterized completely by the two-point frequency−frequency correlation function (FFCF) $\langle \delta\omega(t)\ \delta\omega(0)\rangle$, where $\delta\omega(t) = \omega(t) - \langle\omega\rangle$. Thus, $\omega(t)$ is the time-dependent transition frequency of a given OH oscillator and $\langle\omega\rangle$ is the average

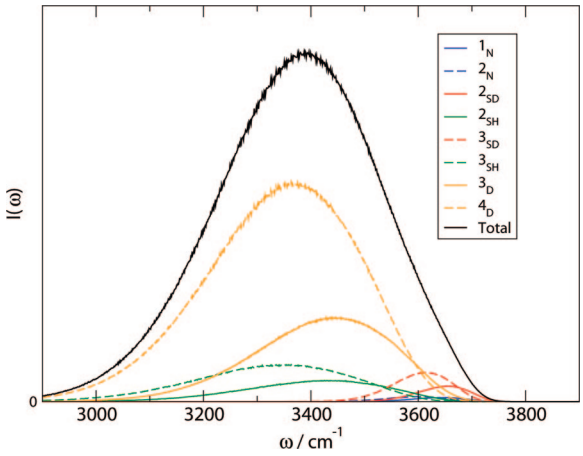

Figure 4. IR spectral density subdistributions for different H-bonding classes, for dilute HDO in D_2O.

frequency of the ensemble. Within the Kubo model, the frequency fluctuations describe a Gauss−Markov process, meaning that the FFCF decays exponentially:

$$\langle \delta\omega(t)\, \delta\omega(0)\rangle = \Delta^2 e^{-|t|/\tau} \qquad (1)$$

Δ^2 is the mean-squared frequency fluctuation, and τ is the correlation time. The FFCF for water is somewhat more complicated (see below); still, one can understand the motional narrowing trend by considering this model. The time scale for frequency fluctuations (τ) is not very different for the HDO:D_2O and HDO:H_2O systems, while Δ is significantly larger in the case of HDO:D_2O. According to the Kubo model, the dimensionless product $\Delta\tau$ determines the extent of motional narrowing. Since this product for HDO:D_2O is larger, there is less motional narrowing. This explains why the observed line width for HDO:H_2O is smaller than one might expect, given the scaling, discussed above, of the gas-phase frequencies and the red-shift. Similarly, there is even more motional narrowing in the HTO:H_2O system.[72]

Finally, we can attempt to address the question about the relationship between H-bonding and vibrational line shapes. To do so, we need a definition of the H-bond. Although this topic is fraught with ambiguities,[128] herein we will use a new ES-based definition developed recently in the Skinner group.[128] Within this approach, each HDO molecule is assigned to one of eight H-bonding classes, according to the total number of H-bonds, the number of donors (H-bonds to the H or D atoms), and, if it is a single donor, whether the donor is the H or D atom. Thus, for example, an HDO molecule in class 2_{SD} has a total of two H-bonds, it is a single (S) donor, and the single donor is the D atom. For the HDO:D_2O problem, Auer et al. decomposed the frequency distribution into subdistributions for each of the eight H-bonding classes.[117] In Figure 4 we do something analogous, but instead we decompose the spectral density (since that is more relevant for the IR spectrum).[126] One sees that the eight distributions fall into two groups, of four classes each. Those lacking an H-bond to the H (1_N, 2_N, 2_{SD}, and 3_{SD}) all absorb between 3450 and 3750 cm^{-1}. On the other hand, those four classes possessing an H-bond to the H (2_{SH}, 3_{SH}, 3_D, 4_D) all absorb in the broad range between 2900 and 3700 cm^{-1}. From this analysis we can say that (within the model!) molecules with a free−OH group do absorb in a relatively narrow frequency range (which, by the way, are the molecules producing the blue shoulder in the Raman spectrum[114]), while molecules without a free−OH (that is, those in the H-bonding region) do not. To reiterate, then, it is not correct to say that molecules in specific H-bonding environments (for example, those in the 4_D, sometimes called "ice-like", class) absorb in relatively narrow frequency ranges.[97,99,117,126] This conclusion seems to be robust to different H-bond definitions[126] (although at present we have no information as to robustness with respect to different water simulation models).

3. Vibrational Spectroscopy as a Probe of Spectral Diffusion

The H-bond dynamics of liquid water play an important role in chemical processes occurring in aqueous media.[120,129] For instance, the formation and breaking of H-bonds between water and reacting molecules can strongly affect the kinetics and energetics of chemical reactions. The dynamics of the H-bond network occur over many time scales, ranging from femtosecond fluctuations that involve a few molecules to picosecond diffusive motions that involve the breaking and formation of H-bonds.[99,103,130,131]

Time-resolved IR spectroscopy is an ideal technique to investigate the dynamics of H-bonds in water, because, as we discussed in the previous section, the frequencies of the intramolecular OH stretching vibrations of a water molecule are particularly sensitive to the molecule's H-bond environment. Generally speaking, the strengthening of the bond will lead to a red shift of the OH frequency, and a weakening will lead to a blue shift of this frequency.[132] Therefore, time-dependent shifts in the OH vibrational frequency, or spectral diffusion, can be used to characterize changes in H-bonding and intermolecular configuration.

Spectral diffusion is most succinctly described by the FFCF, which, within the Kubo model, is a single exponential, as in eq 1. More generally, the time dependence of the FFCF is often modeled as a *sum* of exponentials,

$$\langle \delta\omega(t)\, \delta\omega(0)\rangle = \sum_i \Delta_i^2 e^{-|t|/\tau_i} \qquad (2)$$

each with an amplitude Δ_i^2 and a time constant τ_i.

3.1. Experimental Techniques for Studying Spectral Diffusion

In the recent past, the frequency fluctuations of the OH stretch vibrations have been investigated with nonlinear vibrational spectroscopy. In the following, we will briefly describe and compare the nonlinear techniques that have been used. In all experiments, the femtosecond mid-IR pump and probe pulses are generated via a sequence of nonlinear frequency-conversion processes that are pumped by the output of Ti:sapphire multipass and/or regenerative amplifiers (800 nm, 1 kHz, pulse energy ≥1 mJ). The mid-IR pump has a wavelength of ∼3 μm (≃3300 cm^{-1}) or ∼4 μm (≃2500 cm^{-1}), depending on whether the OH or the OD stretch vibration is being studied. In most studies, the pulses are generated via an optical parametric amplification process in a potassium titanyl phosphate (KTP) or $KNbO_3$ crystal that is pumped by a part of the 800 nm pulses of the Ti:sapphire laser. The energy of the generated pump pulses varies between 2 μJ[133] and 10 μJ.[134−139] In some studies, the KTP and $KNbO_3$ crystals are quite short (1 mm) and the 800 nm

pulses have a pulse duration of 30[105,140] or 40 fs.[133,141] The resulting mid-IR pulses are ultrashort, having a pulse duration of ~50 fs.[105,133,140,141] The bandwidth of these pulses is ~400 cm^{-1}, thereby covering completely the absorption band. In other studies, longer crystals (4−5 mm) and longer 800 nm pulses (~100 fs) have been used, leading to the generation of longer (~150 fs) mid-IR pump pulses with a much narrower spectral bandwidth of ~100 cm^{-1}.[134−137,139]

The pulses are used to excite and probe OH/OD stretch vibrations. As discussed above, isotopically diluted water is studied, probing either the OH stretch vibration of HDO dissolved in D_2O or the OD vibration of HDO dissolved in H_2O. The use of isotopically diluted water has as advantages that the heating effects are limited and, as pointed out in the Introduction, that the signals are not affected by the strong intra- and intermolecular couplings of the OH/OD stretch vibrations of pure H_2O/D_2O.[49] In cases where the stretch vibration of HDO:D_2O is studied, the concentration of HDO is ~1%. When the stretch vibration of HDO:H_2O is studied, the concentration of HDO is somewhat higher, ranging from 2.5 to 4%. In the latter experiments, a higher concentration has to be used, because the H_2O solvent has a non-negligible absorption in the frequency region of the stretch vibration. For either system, the excitation induces a transfer of a few percent of the population of the $v = 0$ ground state of the OD/OH stretch vibration to the $v = 1$ excited state. This transfer leads to a bleaching effect at the fundamental transition frequencies due to a decrease of the $v = 0 \rightarrow 1$ absorption and the presence of the $v = 1 \rightarrow 0$ stimulated emission. The population transfer to $v = 1$ also leads to induced absorption at frequencies corresponding to the $v = 1 \rightarrow 2$ transition. The latter absorption is red-shifted with respect to the fundamental transition by ~220/150 cm^{-1} due to the anharmonicity of the OH/OD stretch vibration.

3.1.1. Spectral Hole Burning

In spectral hole burning, the OH/OD stretch absorption band is excited with a relatively narrow-band mid-IR excitation pulse. If the time scale for spectral diffusion is long compared to the laser pulse duration, the pulse will only excite water molecules in a limited frequency range, leading to a so-called spectral hole in the absorption band. Due to spectral diffusion, the spectral hole will broaden and the central frequency of the hole will shift toward the peak of the absorption band. If the spectral modulation forms a Gauss−Markov process, the shift of the central frequency of the spectral hole shows the same dynamics as the FFCF; that is, this frequency shifts toward the peak with an exponential time dependence, characterized by a time constant τ. The width of the spectral hole broadens with a time constant half as long.

The first studies of spectral diffusion of the OH stretch vibrations of water were performed via spectral hole-burning spectroscopy of the OH stretch of HDO dissolved in D_2O using relatively long mid-IR pulses with pulse durations > 1 ps. From the measurements, it was concluded that the stretch absorption band contains several sub-bands.[87,88] Later studies employing femtosecond pulses did not find evidence for the existence of sub-bands and rather found that the spectral dynamics can be modeled well as a Gauss−Markov process.[142,143]

Figure 5 presents transient absorption spectra of the OH stretch vibration of HDO:D_2O measured with IR pulses with a pulse duration of ~150 fs. Each spectrum is obtained with

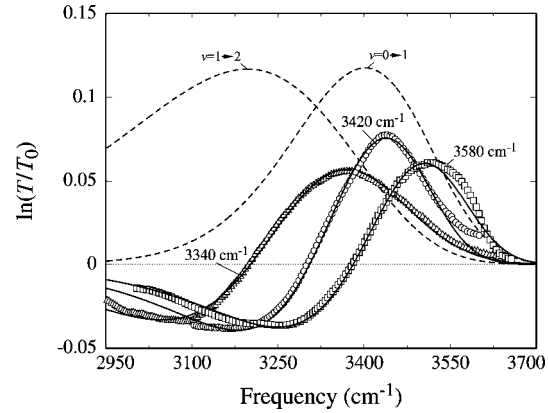

Figure 5. Transient spectra of an aqueous solution of 0.5% HDO dissolved in D_2O obtained with three different pump pulses. The spectra are measured at a delay of 300 fs after excitation by the pump pulse.

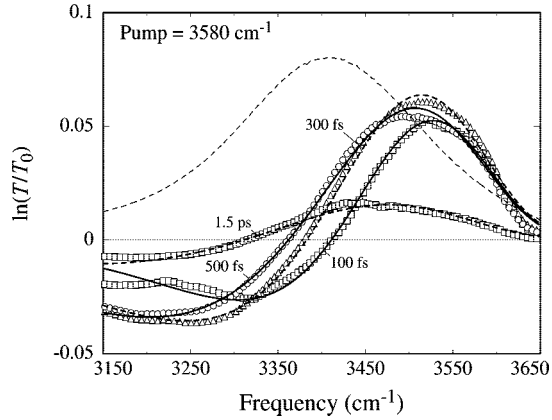

Figure 6. Transient spectra of an aqueous solution of 0.5% HDO dissolved in D_2O at different time delays after excitation with a pump pulse centered at 3580 cm^{-1}.

a different central frequency for the pump pulse. For probe frequencies >3300 cm^{-1}, the signal is positive and results from the bleaching of the fundamental $v = 0 \rightarrow 1$ transition. For frequencies <3300 cm^{-1}, the signal is negative and results from the induced $v = 1 \rightarrow 2$ transition absorption. For all three pump frequencies, the bleaching is narrower than the linear absorption band, which means that the excitation leads to the formation of a spectral hole in an inhomogeneously broadened absorption band. In Figure 6, transient spectra are shown at different delays after excitation in the blue wing of the absorption band. It is seen that the spectrum broadens and that its central frequency shifts toward the maximum of the absorption band. From these spectral dynamics, it was deduced that the FFCF shows a dominant exponential decay component with a time constant of ~1 ps.[142−144]

3.1.2. Photon-Echo Peak Shift Spectroscopy

In photon-echo spectroscopy, the OH stretch absorption band is excited with broad-band IR laser pulses that cover the whole width of the absorption band. The excitation is performed with two pulses, with wavevectors $\mathbf{k}_1$ and $\mathbf{k}_2$, that enter the sample at different angles. As a result, a population grating is excited, with a wavevector corresponding to the difference wavevector of the two excitation pulses. If the absorption band is inhomogeneously broadened, there will be a population grating for each different frequency in the absorption band. The relative phases of these different

frequency gratings will change with increasing delay between the two excitation pulses, because of the differences in the rate of phase evolution of the OH oscillators in the time interval between the two excitation pulses. In the population grating phase (after the second pulse), there is no further phase accumulation. The frequency gratings are read out by a third pulse that has a direction $\mathbf{k}_3$. This third pulse generates a polarization in the directions $\mathbf{k}_3 + \mathbf{k}_2 - \mathbf{k}_1$ and $\mathbf{k}_3 + \mathbf{k}_1 - \mathbf{k}_2$. In the so-called rephasing direction, which is $\mathbf{k}_3 + \mathbf{k}_2 - \mathbf{k}_1$, if the pulse with $\mathbf{k}_1$ enters first, the phase accumulation is opposite to the phase accumulation between the first and second pulses. Hence, the polarizations generated by the third pulse get into phase again after a time delay that corresponds to the time difference between the first two excitation pulses. At that moment in time, all polarizations add up constructively, and a light pulse is emitted from the sample in the rephasing direction. Because the emission is delayed with respect to the entrance time of the third pulse, the emitted light pulse is denoted as a photon echo.

In an echo-peak shift measurement, the delay between the first two excitation pulses that gives the maximum echo signal is measured as a function of the so-called waiting time between the excitation pulses and the third interrogation pulse. In the absence of spectral diffusion and for short waiting times, the maximum photon-echo signal is attained if the first two excitation pulses are somewhat delayed with respect to each other, because this configuration leads to the largest amplitude of the population gratings. However, if there is spectral diffusion and the waiting time is comparable to the characteristic time scale of these processes, the optimal delay between the two excitation pulses will become smaller. This can be understood as follows. If the excitation pulses enter the sample simultaneously, all frequency gratings are excited in phase, and the echo signal is generated directly with the entrance of the third pulse. In this case, changes in the frequencies of the oscillators will not affect their relative phases and there is no rephasing process required to let the polarizations add up constructively. Hence, the echo signal becomes insensitive to the frequency fluctuations. The decay of the optimal time delay between the two excitation pulses as a function of the waiting time constitutes the so-called echo peak signal. For long waiting times, it can be shown that the waiting-time dependence directly represents the time dependence of the FFCF.[145,146]

The spectral diffusion of HDO dissolved in D_2O has been measured with several echo-peak shift spectroscopic studies.[105,140,147] These studies confirmed the presence of a spectral fluctuation process with a time constant of ~1 ps, as was also observed with spectral hole burning. In one study, very slow additional dynamics were observed occurring on a time scale of 5−15 ps.[147] However, in a later study, it was argued that these dynamics likely result from an interference effect with signal generated from the D_2O solvent.[148] In the other echo-peak shift study,[105,140] by Tokmakoff and co-workers, in which 40 fs mid-IR pulses were used, it was observed that there were two different time scales for the spectral modulation. The echo-peak shift resulting from this study is presented in Figure 7. Analysis of the peak shift shows a slow spectral diffusion process with a time constant of 1.4 ps and a fast spectral diffusion process with a time constant of ~50 fs. Moreover, an increase in the FFCF extracted from experiment was observed at a waiting time of ~180 fs. This "recurrence" was assigned to an oscillation associated with the stretching vibration of the bond.[98,103] It follows from this observation that the bond between HDO and a D_2O molecule is underdamped.

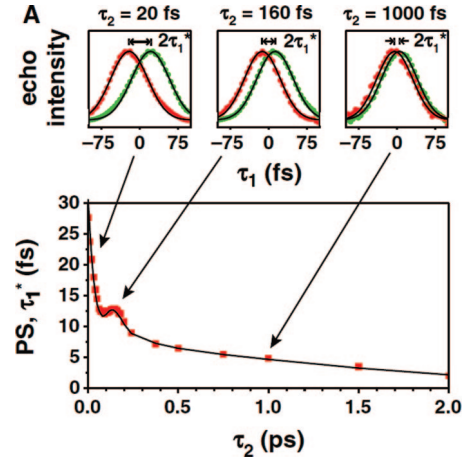

Figure 7. Echo intensity and echo-peak shift as a function of the waiting time τ_2 for HDO:D_2O.[105] Reproduced with permission from ref 105. Copyright 2003 American Association for the Advancement of Science.

3.1.3. Other Photon-Echo Experiments

The first photon-echo studies on water were performed with only two pulses.[149] In these experiments the second pulse serves both to excite and to probe the population gratings. In the experiment the time-integrated echo signal was measured as a function of the delay between the two excitation pulses. This experiment does not give direct information on the time scales of the frequency fluctuation processes, but it does give information on the dephasing time of the OH oscillators. Using certain assumptions, this dephasing time can be related to the time scale of the frequency fluctuations. If the oscillators lose their phase relation in the time interval between the first and second pulses, the generated population grating will not have a well-defined relative phase and there will be no echo signal. Hence, the echo signal will decrease with increasing delay between the two excitation pulses. In such a two-pulse photon-echo experiment, the dephasing time T_2 was measured to be 66 fs < T_2 < 132 fs. This experiment shows that the absorption line of the OH stretch vibrations contains a significant homogeneous component, which indicates the presence of very rapid spectral fluctuations. The time scale of these very rapid spectral fluctuations was estimated to be ~30 fs. The observation of a significant homogeneous broadening component agrees with the findings of the spectral hole-burning studies, in which it was found that the spectral width of the hole is already substantial (>100 cm^{-1}) directly after the excitation (Figures 5 and 6).

In another two-pulse photon echo experiment, the echo signal was time-resolved by interfering this signal with a reference pulse (local oscillator).[150] The delay of the maximum of the echo signal with respect to the second pulse was measured as a function of the delay between the first and second pulses. For a purely inhomogeneously broadened system, the delay of the echo signal would always correspond to the delay between the first and second pulses. In the presence of frequency fluctuations, the delay of the maximum of the echo signal will not exactly follow the increase of the delay between the two excitation pulses, because the frequency fluctuations prevent the full rephasing of the echo signal from occurring. Hence, the maximum echo signal will

occur at a shorter delay after the second pulse. From these experiments it followed that the spectral modulation includes two processes with time scales of 130 and 900 fs. This observation thus agrees reasonably well with the results of the echo-peak shift studies.

3.1.4. Two-Dimensional Vibrational Spectroscopy

Two-dimensional (2D) vibrational spectroscopy is another variation of third-order nonlinear spectroscopy. The name 2D spectroscopy refers to the fact that the signals measured with this technique can be presented in a contour plot as a function of two frequency dimensions, corresponding to the excitation and the probing frequencies. There are two variations of 2D spectroscopy: double-resonance or dynamic hole-burning spectroscopy and pulsed Fourier-transform or heterodyne-detected photon-echo spectroscopy.

Double-resonance spectroscopy is a conventional spectral hole-burning experiment in which a narrow-band pump pulse is scanned through the absorption band. The frequency spectrum of the pump pulse is often produced by passing a short, broad-band pump pulse through a piezocontrolled Fabry−Perot etalon. With the etalon, both the central frequency and the bandwidth can be varied. The probe pulse is a fraction of the broad-band input pulse, and after its transmission through the sample, it is spectrally dispersed and frequency-resolved detected. The main difference with a conventional spectral hole-burning experiment is formed by the adjustable Fabry−Perot filter used to control the pump spectrum before the pump enters the sample.

Heterodyne-detected photon-echo spectroscopy is a three-pulse photon-echo experiment. The generated photon-echo signal is Fourier transformed with respect to two time variables, with the first being the delay time between the two excitation pulses and the second being the time between the echo signal and the third pulse. This technique can be best explained as a multiple hole-burning experiment. Two ultrashort pulses separated by a certain time show a frequency-modulated spectrum with a modulation frequency that is inversely proportional to the pulse delay. This spectral modulation imprints a corresponding population frequency grating in the sample absorption band or, in other words, burns multiple holes in the absorption line. Increasing the time separation between the pulses in the first pair leads to a finer frequency modulation and to more severe smearing of the holes due to spectral diffusion. The dependence of the signal on the excitation frequency is obtained by performing many experiments in which the delay between the two excitation pulses is varied. Fourier transformation of all these signals gives the dependence of the signal on the excitation frequency. An important condition for this procedure is that the phase relation between the two excitation pulses is well-defined. The probing frequency axis is obtained by interferometric superposition of the echo signal with a fourth laser pulse. This fourth laser pulse acts as a local oscillator in a heterodyning experiment. The frequency of the echo signal can be determined in the time domain by scanning the time delay of the local oscillator and Fourier transforming the thus obtained signal with respect to this time variable or by spectrally dispersing both beams in a spectrograph. The outcome of the experiment is dependent on the phase difference between the two excitation pulses and the phase difference between the echo signal and the local oscillator field. Hence, the experiment requires a high mechanical stability.

The two types of 2D spectroscopic experiments give the same type of information. The double-resonance technique has as an advantage that it is relatively simple and that it does not require phase stability. This technique has as a disadvantage that the measured spectral shapes are always convoluted with the prechosen bandwidth of the pump pulse. As a result, fine spectral details (narrow homogeneous lines) could be missed if the prechosen pump bandwidth is too large. The heterodyne-detected echo has as an advantage that it automatically provides the optimal frequency resolution for studying the spectral dynamics. If the spectrum contains very narrow homogeneous lines, the signals obtained with long delay times between the excitation pulses will strongly contribute to the 2D spectrum, meaning that the 2D spectrum indeed will show these fine spectral details.

Both 2D techniques can be used to monitor spectral diffusion of the OH/OD stretch vibrations of water by measuring the signal as a function of the delay between the second and third excitation pulses. For short delays, there is a strong correlation between the frequency at which the OH/OD stretch vibration is excited and the frequency at which it is probed. This means that the spectral contour in the 2D spectrum will be strongly elongated along the diagonal (for which the excitation and the probing frequency are the same). With increasing delay time between the excitation and the probing, the frequency correlation decreases, which leads to a broadening of the spectral contour along the off-diagonal direction. Eventually this contour acquires a circular shape, indicating that the correlation between the excitation and probing frequencies is completely lost. This change in shape is directly connected to the time dependence of the FFCF. Different methods have been developed to relate the time-dependent spectral contour to the FFCF, involving the time dependences of the nodal slope,[151] the dynamic line width,[152] the ellipticity,[153] and the inverse of the center line slope.[154]

2DIR experiments on HDO:H_2O and HDO:D_2O have been performed by the Fayer[152,155,156] and Tokmakoff[151,157,158] groups, respectively. The former experiments were analyzed within the context of the dynamic line width. This is the width of the spectral hole as a function of the time delay between the excitation and the probing process. The dynamic line width can in principle be obtained by taking a cross section of the spectral contour along the probing frequency for a fixed excitation frequency. However, the 2D spectrum will contain not only a spectral contour due to the bleaching of the fundamental $v = 0 \rightarrow 1$ transition but also a contour associated with the excited state $v = 1 \rightarrow 2$ absorption. This latter contour is red-shifted along the probing frequency axis by the anharmonicity of the stretch vibration. As the two contours overlap, the projection of the bleaching signal along the probing frequency axis has to be corrected for the contribution of the excited state absorption. In Figure 8 the dynamic line width is presented, for HDO:H_2O, as a function of the delay between the excitation and probing pulses.[156] The dynamical line width is clearly observed to broaden with increasing time delay, closely following the dynamics of the FFCF. It is also observed that the initial line width is quite large, indicating that the OD absorption line contains a significant homogeneous line broadening component, in agreement with the results of two-pulse photon echo and spectral hole-burning studies. The FFCF extracted from these experiments shows a long-time decay of 1.4 ps.[156] These experiments[155] also showed an interesting frequency dependence: at short times (∼100 fs) the dynamic line width

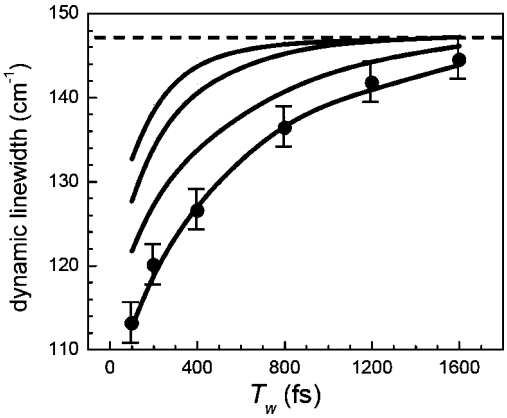

Figure 8. Dynamic line width as a function of the waiting time T_w for HDO:H_2O.[156] Experimental results are the points with error bars, and the solid line going through the points results from a triexponential fit to the FFCF. Also shown are simulation results from the TIP4P (top line), SPC/E (middle line), and SPC/FQ (bottom line) models. The dashed line at 147 cm^{-1} is the long-time asymptotic line width. Reproduced with permission from ref 156. Copyright 2004 American Institute of Physics.

depends on excitation frequency, being wider on the blue side of the line (than at the line center). This demonstrates that molecules on the blue side undergo more rapid spectral diffusion. This was interpreted as resulting from the less constrained environments for water molecules with weaker H-bonds.

An example of the 2DIR line shapes for HDO:D_2O[151,157,158] is shown in Figure 9.[158] These experiments were analyzed with nodal slope[151] and spectral contour ellipticity[157] metrics. The spectral shape changes with increasing waiting time were consistent with the FFCF, as deduced from the earlier peak-shift experiments from the same group.[105,140] These 2DIR line shapes also show rapid and large frequency changes in the blue wing. From the experimental results and computer simulation and theoretical modeling, Tokmakoff and co-workers argue that the rapid spectral diffusion on the blue side indicates that molecules with broken H-bonds are intrinsically unstable; thus, their existence is only "fleeting", lasting less than 150 fs. Most of these broken H-bonds result from excursions from local H-bonded minima, while others occur at the transition state of rapid H-bond switching events. This then has broader implications for the nature of liquid water itself; the authors conclude that "continuum" rather than "mixture" models are more appropriate.[151]

3.2. Theoretical Approaches to Spectral Diffusion Observables

A number of calculations related to spectral diffusion and associated observables in HDO:D_2O or HDO:H_2O have appeared in recent years.[98−106,111,112,115−117,140,151,152,155,156,158−160] All of these studies proceed with the approach outlined in section 2.2: a classical MD simulation of rigid water molecules is run, and one method or another (see section 2.2) is used to determine the OH/OD stretch transition frequency for a given configuration of the classical variables (rotations and translations of all the molecules). This produces a trajectory of the fluctuating transition frequency.

This information can then be used at different levels of theory to compare with ultrafast observables. At the simplest level one assumes the frequency fluctuations are Gaussian, which is equivalent to making a second-cumulant truncation,[122] in which case all information from the frequency trajectory is contained within the FFCF. In addition, it is then possible to obtain the FFCF from different nonlinear experiments. Several such calculations of the FFCF[98−106,111,112,115−117,140,151,158−160] give results that are in qualitative agreement with that extracted from experiment, showing a rapid ∼50−100 fs initial decay, a small oscillation with a period of about 150 fs, and a slower decay of about 0.5−1 ps. The long-time decay is somewhat faster than in experiment (∼1.4 ps), which has been attributed to deficiencies of the nonpolarizable simulation models used for the MD simulation. A follow-up study[160] using the fluctuating-charge simulation model of Rick et al.[161] found a slower long-time decay of the FFCF of ∼1.5 ps, in closer agreement with experiment. This model, however, does not show the experimentally observed oscillation. These calculations confirm the interpretations described earlier, that the short-time decay corresponds to inertial motion along the H-bond stretch coordinate and the oscillation corresponds to underdamped motion near the minimum of the same coordinate. The decay of the FFCF at times on the order of 1 ps occurs on the same time scale as the making and breaking of H-bonds and has been attributed to this process,[99,100,103,104] although Tokmakoff and co-workers have argued that the long-time decay of the FFCF is due to more collective structural relaxation.[105,106,140]

Within the Gaussian approximation one can then use the FFCF to calculate nonlinear response functions and hence ultrafast observables.[122] However, it has come to be appreci-

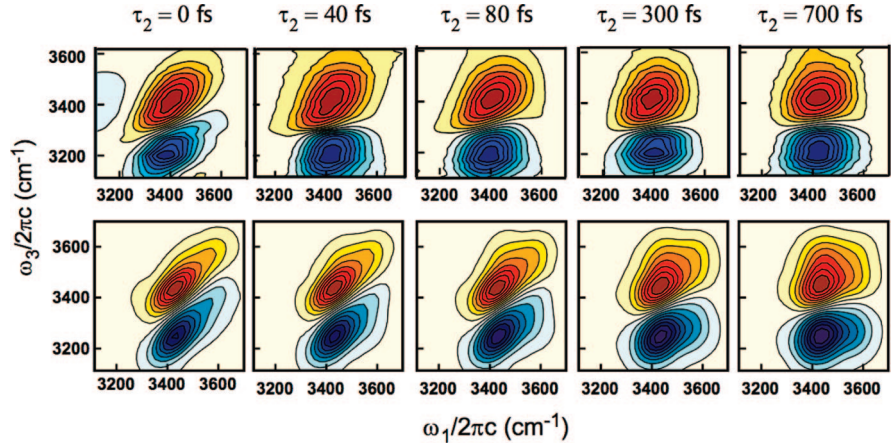

Figure 9. Experimental (top) and simulated (bottom) absorptive 2DIR heterodyne-detected photon-echo spectra of the stretch vibration of HDO:D_2O for several waiting times τ_2.[158] Reproduced with permission from ref 158. Copyright 2006 American Institute of Physics.

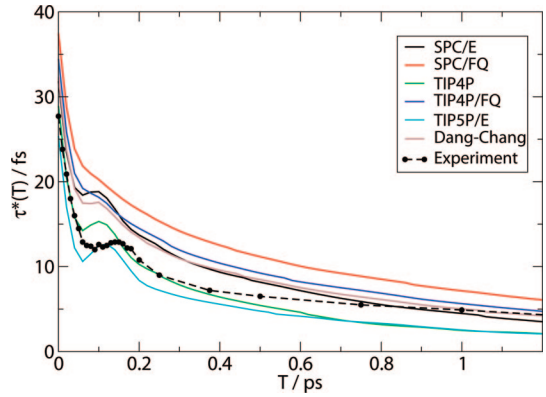

Figure 10. Calculated[116] (for six different simulation models) and experimental[105] echo-peak shifts as a function of waiting time T for HDO:D_2O. Reproduced with permission from ref 116. Copyright 2007 Elsevier.

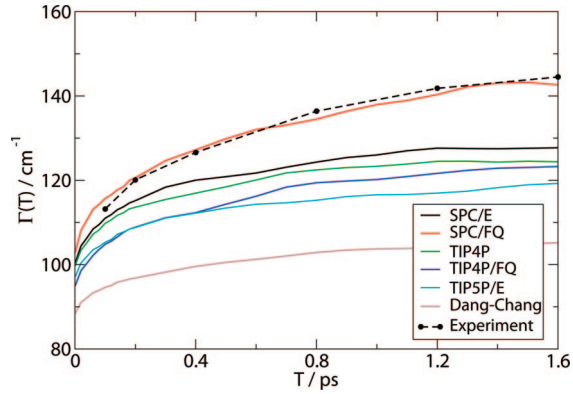

Figure 11. Calculated[116] (for six different simulation models) and experimental[156] dynamic line widths as a function of waiting time T for HDO:H_2O. Reproduced with permission from ref 116. Copyright 2007 Elsevier.

ated theoretically that for water the frequency fluctuations are not particularly Gaussian.[98,101−104,162] This was confirmed experimentally by the asymmetric 2DIR line shapes.[151,152,155−158] One consequence of this is that it then becomes impossible to extract the FFCF from nonlinear experiments. One can avoid this approximation theoretically by calculating the nonlinear response functions directly from the frequency trajectory.[101,102,115−117,151,158,159] One such calculation[102] for the echo-peak shift of HDO:D_2O actually preceded the experiments of Fecko et al.,[105] showing qualitative agreement, including the underdamped oscillation. Similar calculations for 2DIR spectra have also appeared[115−117,151,158] and have been used, for example, to support arguments for the "fleeting" nature of non-H-bonded configurations (see Figure 9, bottom panel).[151,158]

At the next level of theory one can include non-Condon effects,[114−116] by determining the trajectory of the fluctuating dipole moment as in section 2.2 and including that in the calculation of nonlinear response functions. These non-Condon effects (occurring because the magnitude of the vibrational transition dipole depends on bath coordinates such as H-bonding distances) are moderately important for the IR and Raman line shapes in water[114] and somewhat more important for nonlinear experiments.[115] In particular, for pump−probe, spectral hole-burning, and heterodyned photon-echo experiments, the signal goes like the fourth power of the transition dipole, whereas for homodyned photon echoes it goes like the eighth power.

With the large variety of linear and nonlinear vibrational spectroscopy experimental results available for liquid water, and the presence of presumably reasonably reliable frequency and transition dipole maps, one wonders whether experiment can be used to assess the reliability of classical simulation models for water. Thus, in a combined theoretical and experimental study,[116] spectroscopic observables were calculated for six different popular simulation models; we included non-Condon effects, non-Gaussian frequency fluctuations, vibrational relaxation, rotations, and convolutions over the experimental pulse envelopes, and the results were compared with line shape, echo-peak shift, and 2DIR experiments (nodal slope and dynamic line width metrics). In Figure 10 we show experimental[105] and calculated (for the six different simulation models) echo-peak shifts for HDO:D_2O. One sees that some models produce the correct initial peak shift, some produce the short-time oscillation, and some produce the correct time constant for the long-time decay, but none do all three! In Figure 11 we show experimental[156] and calculated dynamic line widths for HDO:H_2O. In this case one sees that one simulation model (SPC/FQ[161]) is in good agreement with experiment, while the rest are not. Thus, the conclusions are, in fact, not very conclusive: that all of the simulation models gave results in qualitative agreement with the experimental results; for individual experiments some models are definitely better than others; and no model performed well for all observables.[116] Overall, the nonpolarizable SPC/E model[113] gave perhaps the best agreement with experiment, although the authors' final conclusion is that "the endorsement of the SPC/E model is also not meant to diminish the importance of polarizability, which is certainly expected to be essential when dealing with inhomogeneous systems (such as the liquid/vapor interface) or aqueous solution".[116]

4. Vibrational Spectroscopy as a Probe of Rotational Dynamics

Molecular reorientation in liquid water has been studied with several experimental techniques, such as NMR,[26−31] dielectric relaxation,[32] THz absorption spectroscopy,[39,40] optical Kerr effect,[163] and quasi-elastic neutron scattering.[38] These experiments are related to the first- and second-rank Legendre polynomial orientational TCFs $C_n(t) = \langle P_n(\hat{u}(t)\cdot\hat{u}(0))\rangle$, with $n = 1$ and 2, respectively, for different molecule-fixed unit vectors $\hat{u}$. With NMR it was found that the correlation time (total integral) of the second-rank TCF (hereafter called the anisotropy correlation function or ACF) for the intramolecular H−H vector is approximately 2.5 ps.[27−30,164,165] Experiments on isotopic mixtures allow for the measurement of correlation times of other (OH and out-of-plane) molecule-fixed unit vectors, the latter of which turns out to be about 25% shorter, showing that the rotational motion of water is not isotropic.[26] With dielectric relaxation and THz absorption, fluctuations of the total dipole moment of the sample are probed, yielding a Debye time of ∼8 ps for room temperature liquid water.[32,39,40] It is difficult to make a straightforward comparison between these numbers for several reasons: (1) the NMR values are correlation times, as described above, while the Debye value is a "relaxation" time (characterizing long-time exponential decay). If the decay of a TCF is nonexponential at short times, these two times will be different. (2) NMR times describe rotational properties of single molecules, while Debye relaxation is a collective process. (3) NMR times are for the second-rank

TCF, while Debye relaxation is for the first-rank TCF. (4) NMR times are for three different molecule-fixed unit vectors, none of which is in the direction of the molecule's dipole (which is probed by Debye relaxation).

Ultrafast IR spectroscopy can measure the second-rank orientational dynamics of the OH bond vector of individual molecules.[133−141] One advantage of the IR experiment is that the full ACF can be measured (whereas the NMR experiment measures only the integrated correlation time). In addition, through excitation and probing with different light frequencies, IR experiments have the possibility to measure the reorientation of different subensembles.

The measurement of the orientational dynamics of water via the excitation of the OH/OD stretch vibrations relies on the fact that the rotation of the molecule changes the direction of the vibrational transition dipole moment. This method does not work if there are other processes contributing to the change of the direction of the transition dipole moment, such as intramolecular and/or intermolecular resonant (Förster) energy transfer between the vibrations. As a result, it is unfortunately not possible to measure the orientational dynamics of the molecules in pure liquid H_2O.[49] Consequently, the reported femtosecond mid-IR measurements of the orientational dynamics of water always refer to HDO molecules dissolved in either normal or heavy water.[133−144] In both cases the dynamics of a hydroxyl group (either OH or OD) embedded in a network of isotopically distinct hydroxyl groups are studied. Studying the orientational dynamics of the stretch vibration of HDO:D_2O has the advantage that it is easier to resolve dynamical inhomogeneities, as the OH stretch vibration of HDO:D_2O is more strongly inhomogeneously broadened than the OD vibration of HDO:H_2O.[147,152] On the other hand, studying the OD vibration of HDO:H_2O has the advantage that the lifetime of the OD vibration is more than two times longer than that of the OH vibration, thereby allowing the measurement of the orientational dynamics of the OD group over a significantly longer time interval.

4.1. Polarization-Resolved Pump−Probe Spectroscopy

The orientational dynamics of the OH/OD stretch vibrations of HDO dissolved in D_2O/H_2O have been studied with polarization-resolved pump−probe spectroscopy.[43,133−141] The required femtosecond mid-IR laser pulses at wavelengths of $\sim$3 μm ($\simeq$3300 cm^{-1}) or $\sim$4 μm ($\simeq$2500 cm^{-1}) are obtained via similar nonlinear frequency conversion processes, as were briefly described in the previous section. The probe pulses are often obtained by splitting off a small fraction of the pump pulse.[133,134,138−140] In some experiments, independently tunable probe pulses are generated by a separate sequence of nonlinear frequency-conversion processes.[43,135−137]

The rate of molecular reorientation of the water molecules is studied by measuring the time dependence of the anisotropy of the excitation of the OH/OD stretch vibration. In most experiments, the polarization of the pump is rotated before the sample at 45° with respect to the probe polarization with a $\lambda/2$ plate. After the sample, the polarization components of the probe parallel and perpendicular to the pump polarization are alternatingly chosen using a polarizer.[134,135,137−141] In one study[133] the experiment is performed with a probe pulse that has a polarization that is parallel to the pump polarization, and a probe pulse with a polarization at the magic angle (54.7°) with respect to that of the pump.

The signals measured are the ratios of the transmitted probe and reference beams: $T_{||} = I_{||}/I_{ref}$, $T_{\perp} = I_{\perp}/I_{ref}$, and $T_{iso} = I_{iso}/I_{ref}$, where I_{iso} represents the signal measured by a probe pulse with its polarization at the magic angle. To determine the pump-induced changes $T_{||}$, $T_{\perp}$, and T_{iso}, the signals are alternatingly measured with and without the pump pulse present using a 500 Hz chopper in the pump beam. The signals are used to construct the absorption changes $\Delta\alpha_{||} = \ln[T_{||}/T_0]$, $\Delta\alpha_{\perp} = \ln[T_{\perp}/T_0]$, and $\Delta\alpha_{iso} = \ln[T_{iso}/T_0]$, where T_0 represents the transmission signal in the absence of the pump. From $\Delta\alpha_{||}$ and $\Delta\alpha_{\perp}$, the rotational anisotropy can be constructed:

$$R(t) = \frac{\Delta\alpha_{||} - \Delta\alpha_{\perp}}{\Delta\alpha_{||} + 2\Delta\alpha_{\perp}} = \frac{\Delta\alpha_{||} - \Delta\alpha_{\perp}}{3\Delta\alpha_{iso}} \quad (3)$$

The anisotropy can also be obtained from $\Delta\alpha_{||}$ and $\Delta\alpha_{iso}$:[133]

$$R(t) = \frac{\Delta\alpha_{||} - \Delta\alpha_{iso}}{2\Delta\alpha_{iso}} \quad (4)$$

The denominator of eqs 3 and 4 is not affected by the reorientation. Hence, isotropic effects such as vibrational relaxation are divided out. Thus, $R(t)$ is directly related to the ACF:[166]

$$R(t) = \frac{2}{5}C_2(t) = \frac{2}{5}\langle P_2(\cos\theta(t))\rangle \quad (5)$$

where $P_2(x)$ is the second Legendre polynomial and $\theta(t)$ is the angle between the OH/OD bond vectors at time 0 and time t.

4.1.1. Isotropic Absorption Changes

In Figure 12 the isotropic absorption changes are shown as a function of the delay between pump and probe for three different probe frequencies.[43] At probe frequencies of 3400/2500 cm^{-1}, the signal is dominated by a decaying bleach, whereas at 3170/2380 cm^{-1} the signal consists of a decaying induced absorption. In between these two frequencies, more

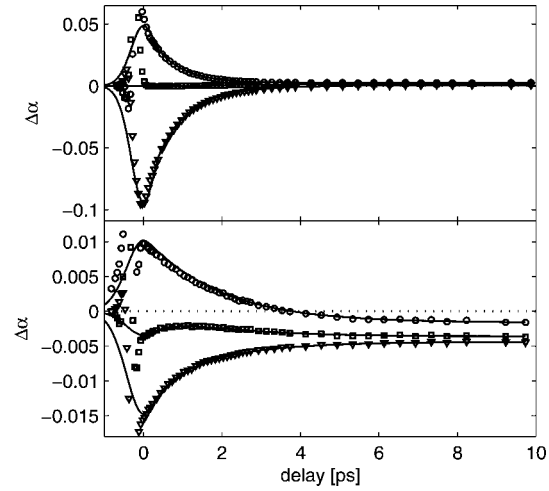

Figure 12. Absorption change as a function of delay between pump and probe for a pump pulse at 3400/2500 cm^{-1} (upper/lower panel) exciting the OH/OD stretch vibration of HDO dissolved in D_2O/H_2O.[43] Shown are transients for probe frequencies of 3170/2380 cm^{-1} (circles), 3250/2430 cm^{-1} (squares), and 3400/2480 cm^{-1} (triangles). Reproduced with permission from ref 43. Copyright 2008 American Chemical Society.

complicated dynamics are observed, especially for the OD vibration. For a probe frequency of 2430 cm^{-1}, a bleaching signal is observed that shows a decay followed by a rerise to a constant (bleached) end level. The latter ingrowing part of the signal reflects the temperature increase of the sample in the focus of the pump beam. The fact that the signal turns over shows that the temperature rise takes place on a slower time scale than the relaxation of the stretch vibration, which implies that the vibrational relaxation proceeds via a nonthermal intermediate state. With MD simulations it was found that the relaxation of the vibration of HDO:D_2O is dominated by energy transfer to the overtone of the bending mode.[78,80,167] This overtone subsequently rapidly relaxes to the first excited state of the bending mode. Hence, the intermediate level is likely formed by the first and/or second excited state of the bending mode of the HDO molecule.

At longer delays (>3 ps) transmission changes are observed that persist over the experimentally accessible time range (500 ps) and that have the character of a bleach on the red side of the spectrum and of an induced absorption on the blue side. These persistent transient spectra reflect the temperature rise in the sample that results from the absorption and thermalization of the energy of the pump pulse. A rise in temperature induces a blue shift and a decrease in cross section of the OH/OD vibrations.[133,138,139] The thermal signal observed at large delays is isotropic, meaning that the magnitude of this signal is the same for $\Delta\alpha_{\parallel}$ and $\Delta\alpha_{\perp}$. Hence, to obtain the anisotropy of the excited OH/OD vibration, the time-dependent thermalization signal has to be subtracted from $\Delta\alpha_{\parallel}$ and $\Delta\alpha_{\perp}$. To determine the delay dependence of the thermalization signal, the spectral responses of the OH and the OD vibration are fitted to a relaxation model.[133,139,168] In this model the relaxation proceeds with time constant $\tau_1 = 1/k_1$ to an intermediate state. This latter state relaxes with time constant $\tau_* = 1/k_*$ to the final state, in which the energy has become thermal. The two time constants τ_1 and τ_* are treated as global fit parameters, and the cross sections of the transitions between the vibrational levels are allowed to vary over the spectrum. The resulting fits are represented by the solid lines in Figure 12. It is seen that the model provides an accurate description of the data, which implies that spectral diffusion effects do not play an important role after a delay of 0.4 ps for pump pulses that are resonant with the center of the absorption bands. For the OH stretch vibration of HDO dissolved in D_2O, $\tau_1 = 0.7 \pm 0.1$ ps and $\tau_* = 0.6 \pm 0.1$ ps. For the OD stretch vibration of HDO dissolved in H_2O, $\tau_1 = 1.8 \pm 0.2$ ps and $\tau_* = 0.9 \pm 0.1$ ps.

4.1.2. Long-Time Results: Collective Orientational Dynamics

Figure 13 shows the anisotropy of the OD stretch vibration of HDO dissolved in H_2O measured as a function of delay for a pump frequency of 2500 cm^{-1} and three different probe frequencies. The anisotropy signals shown are obtained by correcting the measured $\Delta\alpha_{\parallel}$ and $\Delta\alpha_{\perp}$ for the thermalization signal as determined from the isotropic data. An exponential fit to the data shown in Figure 13 yields a time constant of 2.5 ± 0.2 ps at all probe frequencies, in agreement with earlier results.[139,141,169]

The reorientation time constant of the OD vibration of HDO in H_2O (2.5 ± 0.2 ps) is observed to be somewhat shorter than that of the OH vibration of HDO in D_2O (3 ± 0.3 ps).[135−140] At first sight it may seem surprising that the orientational relaxation of the OD group proceeds faster than

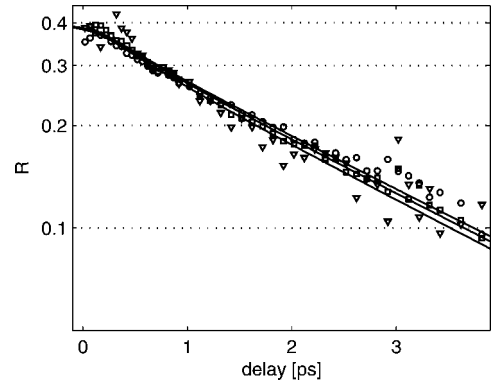

Figure 13. Anisotropy of the OD stretch vibration of HDO dissolved in H_2O as a function of delay between pump and probe for a pump frequency of 2500 cm^{-1} and probe frequencies of 2500 cm^{-1} (circles), 2550 cm^{-1} (squares), and 2600 cm^{-1} (triangles).[43] Reproduced with permission from ref 43. Copyright 2008 American Chemical Society.

that of the OH group, as its moment of inertia is almost twice as large. However, there exist two regimes for the reorientation. On very short time scales (<200 fs), the OH/OD group can show a limited free rotation (libration) while keeping the donated H-bond intact. This regime will be discussed in the following subsection. On longer time scales, which are of relevance here, the orientational dynamics of the groups require rearrangements of the water network.[108,170] In this regime the orientational dynamics are no longer determined by the moment of inertia but instead are governed by the relative motions of the water molecules and, in particular, by the dynamics of H-bond breaking and reformation. A good measure for the translational mobility of the water molecules is provided by the value of the viscosity. Using the viscosities of H_2O and D_2O (0.9 mPa s and 1.1 mPa s, respectively), the reorientation times of the OH and OD are estimated to show a ratio of 0.8, which is very similar to the measured ratio of the reorientation time constants. It should be noted that this finding does not imply that the orientational motion of the water molecules is diffusive. In fact, in a recent molecular dynamics study it was shown that the reorientation involves fast and large angular jumps between different H-bond configurations.[170] The scaling with the viscosity thus likely follows from the fact that the rate-limiting steps of the reorientation are formed by (translational) molecular motions, of which the rate is well characterized by the viscosity.[171]

The measured molecular reorientation times of 2.5/3 ps in H_2O/D_2O agree reasonably well with the results obtained with other techniques. NMR studies arrive at a reorientation time of the water molecule of about 2.35−2.5 ps in liquid H_2O at 298 K[27,30,31] and 2.4−2.9 ps in liquid D_2O at 298 K.[26,30] Note that the values from Jonas et al.[30] are obtained by interpolation using an Arrhenius expression, from the measured results at 283 K and 303 K. Here again one should remember that, for the IR pump−probe experiments and the deuterium quadrupolar relaxation experiments in D_2O,[26] the relevant molecule-fixed unit vector is the OH/OD bond vector, while in the proton NMR experiments on H_2O it is the H−H intramolecular unit vector.[27,30] Therefore, in this case we can make a direct comparison between the two D_2O experiments (and even here one should keep in mind that the IR experiments actually measure the reorientation of HOD in D_2O). One must also emphasize again that the NMR experiments measure the integrated correlation time, whereas

the IR experiments measure the long-time decay. If the ACF is not exponential, these two are not the same. Both experiments and simulation (see below) show, in fact, that the ACF has a very fast drop at short times, whose amplitude is about 10−20% of the initial value, meaning that the NMR time (2.4−2.9 ps) should be about 10−20% shorter than the IR time (3 ps); this is indeed observed to be the case for D_2O.

In comparing the results of femtosecond pump−probe and NMR experiments with the results of dielectric relaxation studies and THz absorption, it should be emphasized again that these techniques measure different orientational TCFs. Femtosecond pump−probe and NMR experiments probe the (second-rank) ACF, whereas τ_D as measured in dielectric relaxation and THz absorption spectroscopy is related to the first-rank TCF. And again we mention that for dielectric and THz spectroscopy the relevant unit vector is different from that in both the NMR and IR experiments (in this case it is along the molecular dipole moment). In dielectric relaxation studies of liquid water, a main relaxation component with a time constant τ_D of 8.3 ps was found.[32] Similar values were found in THz spectroscopic studies of H_2O and D_2O:[39,40] at room temperature the Debye times τ_D of the slow component were determined to be 8.5 ps for H_2O and 10 ps for D_2O. To arrive at the time constant τ_1 of the decay of the first-rank TCF, the values of τ_D have to be corrected for collective effects. This correction is not without ambiguity, but using the approach proposed by Wallqvist and Berne,[172] one arrives at values of τ_1 of 7.6 and 9 ps for H_2O and D_2O, respectively. When comparing these values with the second-rank time constants (2.5 and 3 ps, respectively), one finds ratios that are close to 3. The ratio between the first- and second-rank decay times τ_1 and τ_2 is determined by the nature of the reorientation mechanism. In the case of pure (small step) rotational diffusion $\tau_1 = 3\tau_2$, but if the reorientation takes places via, for example, jump diffusion, this ratio can be lower.[170] In addition to the main component with τ_D, dielectric relaxation and THz absorption studies report a weaker and much faster component with a time constant on the order of 100 fs.[39,40] The origin of this fast component will be discussed in the following subsection.

4.1.3. Ultrashort-Time Results: Librational Motions

In Figure 14 the anisotropy of the OH stretch vibration of HDO:D_2O is shown as a function of delay time up to 1.5 ps.[140,173] This measurement is performed with mid-IR pulses with a pulse duration of 45 fs. The figure clearly shows that the anisotropy decay takes place on two distinctly different time scales. The anisotropy shows a rapid partial decay in the first 100 fs. This decay is interpreted as being due to librational (hindered rotational) motion. Here it should be noted that in these experiments[140,173] the signals measured show little contribution from coherent artifacts because the sample used is a free-flowing water jet. The fast decay is followed by the much slower dominant decay component with a time constant of ∼3 ps.[135−137]

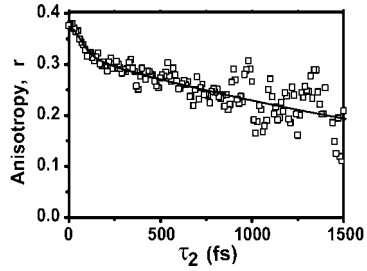

Figure 14. Anisotropy of the OH stretch vibration of HDO dissolved in D_2O as a function of delay,[173] measured with ultrashort (45 fs), broad-band (400 cm^{-1}) pump and probe pulses with a central frequency of 3400 cm^{-1}. The anisotropy shows a biexponential decay with a fast component in the first 200 fs. Reproduced with permission from ref 173. Copyright 2004 American Physical Society.

The rotational motion observed at short times is, presumably, hindered by the much more slowly rearranging H-bond network. Earlier in the review we discussed how molecules in different H-bonding environments absorb at different frequencies and, in particular, that molecules on the red side of the band have weaker H-bonds than molecules on the blue side. It follows, then, that the short-time dynamics might well be frequency-dependent. Such experiments can be performed with relatively long pulses by pumping and probing at different frequencies in the band.[43,134,136,137] Alternatively, one can use a shorter broad-band probe pulse and then frequency-resolve the signal.[43] Finally, one can use shorter pump *and* probe pulses, whose bandwidths span the absorption line and then frequency-resolve the transient absorption.[141]

The first experiments showing a frequency-dependent anisotropy[134,136] used the narrow-band pump−probe technique and were performed on HDO:D_2O. In these two studies, pump and probe frequencies were chosen to be the same, but the frequency of the pair of pulses was varied throughout the band. The anisotropy decay was distinctly frequency-dependent for times up to 1.5 ps, with faster decays for bluer frequencies, but the decay times for longer times were identical.[136] An interpretation[100] of the experiment was that on the blue side of the line the restraining potential due to H-bonding is weaker, and so the angular excursions at short times will be greater (see below). At times longer than the spectral diffusion time, frequency memory is lost, and so all members of the ensemble decay at the same rate.[100] Related two-color (different pump and probe frequencies) experiments on the same system by Gallot et al.[137] showed similar results.

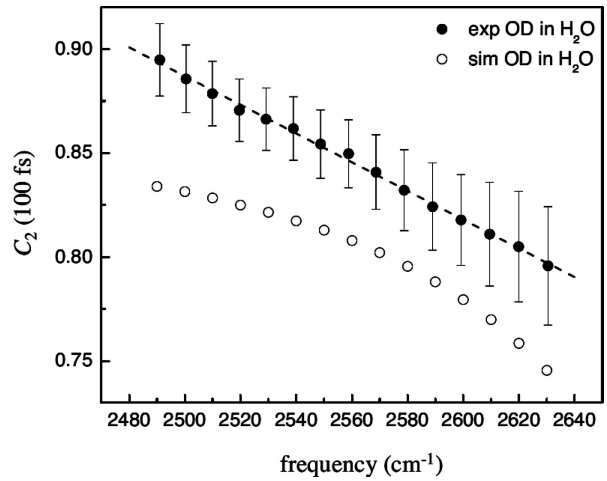

Figure 15. C_2(100 fs) versus OD stretch (probe) frequency for HDO:H_2O.[141] The dashed line is a linear fit to the data (filled circles). The open circles represent calculations from MD simulations (see section 4.2). Reproduced with permission from ref 141. Copyright 2008 National Academy of Sciences.

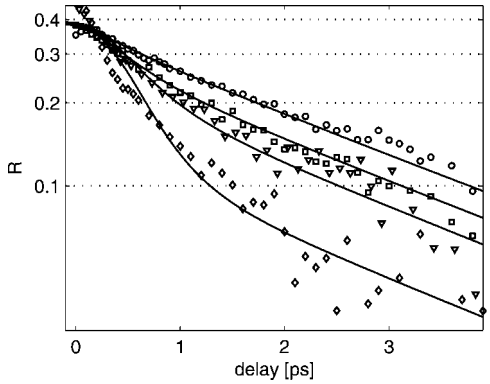

Figure 16. Anisotropy of the OD stretch vibration of HDO dissolved in H_2O as a function of delay,[43] for the same pump and probe frequency of 2500 cm^{-1} (circles), 2550 cm^{-1} (squares), 2600 cm^{-1} (triangles), and 2650 cm^{-1} (diamonds). Reproduced with permission from ref 43. Copyright 2008 American Chemical Society.

As mentioned above, better time and frequency resolution can be achieved with shorter pump and probe pulses, and then frequency-resolving the transient absorption.[141] Fayer and co-workers studied the HDO:H_2O system using this approach, finding that the value of $R(t)$ at $t = 200$ fs varied by about 10%, depending on probe frequency. Considering that the ultrafast inertial component is over by about 100 fs,[140,173] they then extrapolated their results backward to 100 fs and plotted the value of C_2(100 fs) as a function of probe frequency; the results are shown in Figure 15. One sees that the initial drop of the ACF varies from about 10% to about 20% as one goes from the center of the band to the blue edge. One interesting aspect of this work involves the temperature dependence of this frequency-dependent initial drop. At 65 °C the drop varies from 8% to 32%, while at 1 °C the drop is almost constant at about 15%. This last feature is interpreted as indicating that motion just above the freezing point is more collective, and so the strength of the angular potential is not a single-molecule property, explaining the lack of a frequency dependence.[141]

4.1.4. Short-Time Results: Jumping Molecules

Narrow-band pump/broad-band probe experiments, recently performed by Bakker et al.,[43] provide separate pump and probe frequency resolution, albeit at the expense of some time resolution (due to the relatively long pump pulse). These experiments can shed light on the mechanism of molecular reorientation. For example, results[43] for identical pump and probe frequencies, on the HDO:H_2O system, are shown in Figure 16. One sees that the measured anisotropy shows an additional relatively fast component if the OD absorption band is *both* excited and probed in the blue wing. It should be noted that this additional faster decay cannot be caused by librations. The partial decay of the anisotropy due to librations is nearly complete after 100 fs,[108,140] whereas the dynamics observed in the blue wing of the stretch vibration are much slower, having a time constant of ~700 fs.

Results for different pump and probe frequencies[43] are shown in Figure 17. When the OD stretch vibration is pumped close to its central frequency (upper panels), the anisotropy is nearly the same at all probe frequencies, except in the frequency region where the bleaching changes into an induced absorption. In this frequency region the signal results from the competition of these two signals, which leads

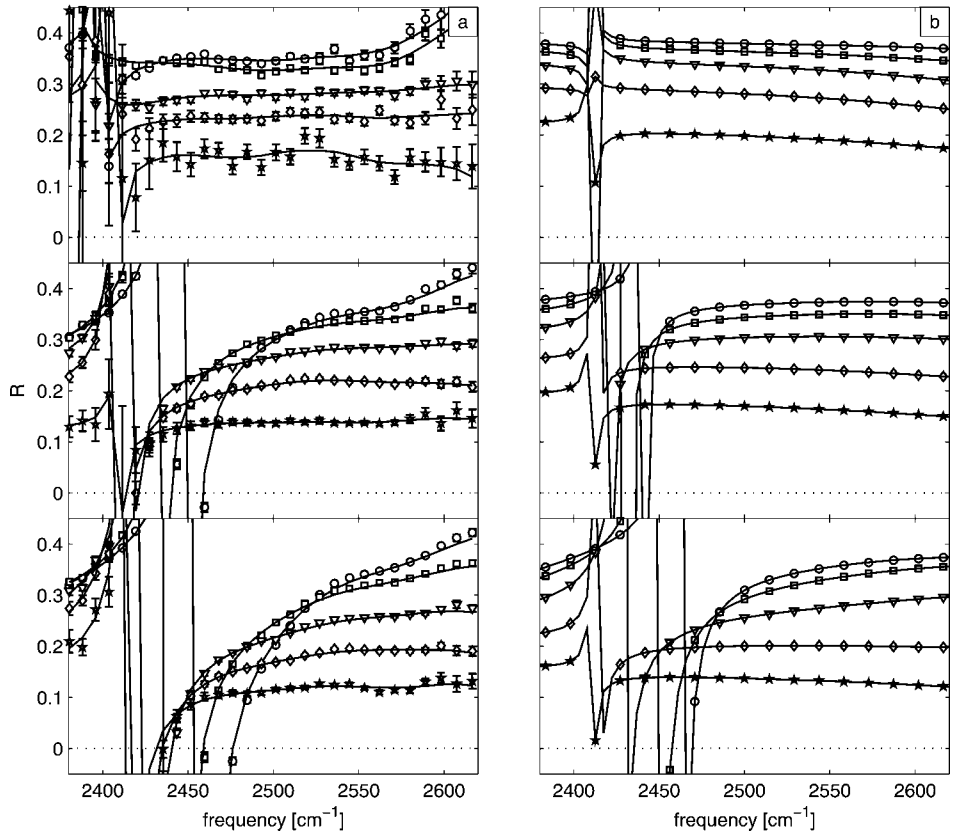

Figure 17. Anisotropy as a function of frequency at delays of 0.1 ps (circles), 0.2 ps (squares), 0.5 ps (triangles), 1 ps (diamonds), and 2 ps (stars). Shown are results obtained with a pump frequency of 2450 cm^{-1} (upper panel), 2550 cm^{-1} (middle panel), and 2650 cm^{-1} (lower panel). Part a shows the experimental results (solid lines are guides to the eye), and part b presents calculated results.[43]

to an erratic behavior of the anisotropy. With increasing delay, the anisotropy decay shows the same decay dynamics at all probe frequencies. When the pump frequency is tuned to the blue wing of the absorption spectrum (lower panels of Figure 17), the anisotropy is observed to become strongly frequency dependent in the first few picoseconds. An interesting observation is that the anisotropy in the center and the red wing is significantly lower than 0.4, already at a delay of 0.2 ps. This observation shows that, directly after the excitation, the signals in the center and in the red wing contain a significant contribution of water molecules that have reoriented.

The low value of the anisotropy in the center and the red wing following excitation in the blue wing is not due to a high intrinsic reorientation rate of molecules absorbing in the center and the red wing. The upper panels of Figure 17 clearly show that water molecules absorbing in the center and the red wing in fact show a slow reorientation. Therefore, the large fraction of reoriented molecules in the center and the red wing *following excitation in the blue wing* must be due to excited molecules that reorient while rapidly changing their frequencies from the excited blue wing to the center and the red wing of the absorption band. This finding closely agrees with the molecular jump model for reorientation that was developed by Laage and Hynes based on MD simulations.[170] In this model, the reorientation involves the breaking of the old H-bond and the formation of a new H-bond, which leads to a large and abrupt change in the frequency of the OD vibration. If the pump pulse is tuned to the blue wing of the absorption band, there will be few molecules directly excited in the center and the red wing of the absorption band. As a result, the relative contribution to the signal of molecules that have reoriented and undergone a large frequency change will be relatively large at these frequencies, leading to a low anisotropy already at early delays. A significant part of the frequency changes takes place within 100 fs, as no initial fast anisotropy decay could be resolved in the center and the red wing of the absorption band. In the blue wing of the absorption band, the number of directly excited molecules is large and the *relative* contribution of molecules that have reoriented and sampled all possible frequencies in the absorption band will be small. Hence, in the blue wing the initial anisotropy is high. Descriptions of model calculations, shown in the right panels of Figure 17, as well as more detailed comparison between these pump−probe results and the predictions of the Laage/Hynes picture,[108,170,171] can be found in the recent Feature Article by Bakker et al.[43]

4.2. Theoretical Approaches to Rotational Anisotropy Observables

The above experimental results show a number of intriguing features for which molecular interpretations are desirable. These include the nonexponential decay of $C_2(t)$, especially the very rapid initial drop and the frequency dependence of its amplitude, and the eventual frequency-independent long-time decay.

As discussed above, small-amplitude librations can occur without large-scale rearrangement of the H-bond network, which leads naturally to the wobbling-in-a-cone model.[43,108,166,169,171] The idea is that a restraining angular potential due to H-bonding restricts the angular motion at short times to explore angles within a cone of semiangle θ_o. At such time τ when the cone is fully explored, the value of the ACF drops to[166]

$$C_2(\tau) = \left[\frac{1}{2}\cos\theta_o(1 + \cos\theta_o)\right]^2 \quad (6)$$

Thus, within this model, from the initial drop of the ACF one can determine the cone semiangle θ_o.[43,108,169] For example, if one assumes that the cone is fully explored at a time τ such that $C_2(\tau) = 0.9$, $\theta_o = 15°$, while if $C_2(\tau) = 0.75$, $\theta_o = 24°$, etc. Estimates for τ range between about 100 and 200 fs,[108,140,141] and estimates for the cone semiangle range from about 15° to 35°.[43,108] In passing, we note that experimental estimates of cone semiangles appear to be somewhat larger for the OH ACF than for the OD ACF.[43] This is perhaps due to larger librational quantum effects[19−24] in the former case (where the relevant reduced mass is presumably lighter, and so the angular extent of the wave function is greater).

Moilanen et al. have generalized the wobbling-in-a-cone model to a harmonic cone model.[141] Thus, instead of free angular motion within a cone, there is motion within an angular harmonic potential characterized by frequency ω. Within this model the angular drop in the ACF, at such time τ that the distribution within the angular potential has attained thermal equilibrium, can be related to the cone frequency. Taking τ to be 100 fs, this analysis yields frequencies ω from 320 to 450 cm^{-1} as the probe frequency goes from the blue edge to the middle of the band (for HDO:H_2O). Smaller (larger) estimates for τ would lead to smaller (larger) initial drops, which would lead to higher (lower) frequencies. In any case, the estimated cone frequency at the middle of the band is in qualitative agreement with the estimated librational frequency (585 cm^{-1}) for HDO:H_2O.[141] Note that the lowest frequency of 320 cm^{-1} has a period of about 100 fs, which is only consistent with equilibration within 100 fs if the libration is strongly damped.

$C_2(t)$ for various molecule-fixed unit vectors has been calculated for many simulation models of liquid water. Relevant to this section are recent calculations using the TIP4P[174] or SPC/E[113] simulation models for the OH bond unit vector.[26,97,100,108,140,141] All of the results show a fast decay within 50 fs, followed by a recurrence at between 60 and 80 fs and then followed by an approximately exponential decay with a time constant on the order of 1.5 ps (for the TIP4P model)[100] or about 2.5 ps (for the SPC/E model).[26,97,108,140,141] The recurrence has been interpreted as arising from underdamped librational motion. This recurrence has not been observed experimentally, possibly due to difficulties arising from coherent artifacts at such short times.

The frequency dependence of the initial drop was first studied theoretically by Lawrence and Skinner.[100] They calculated $C_2(t)$ for HDO:D_2O using the TIP4P water simulation model, but only those molecules whose OH stretch frequency was in a specified frequency window at $t = 0$ contributed to the average. This was intended to represent the frequency selection in a narrow-band pump−probe experiment. The results showed a frequency-dependent initial drop, followed by the above-described recurrence and then followed by a frequency-independent exponential decay with a time constant of about 1.4 ps. The agreement with the experimental data available at the time[136] was only very qualitative. Lawrence and Skinner argued that at longer times—those longer than the spectral diffusion time—the decay rate of $C_2(t)$ becomes frequency independent, as molecules have lost memory of their initial frequency.[100]

In the earlier experiments[136] the OH stretches were pumped and probed at the same frequency. Thus, the calculation of

$C_2(t)$ should have included only those molecules whose OH stretch frequency was in a specified window at time 0 *and* time *t*. This shortcoming was corrected in a more recent paper by Laage and Hynes,[108] where they calculated $C_2(t)$ for different frequencies for HDO:D_2O using the SPC/E simulation model. Their results are similar to the earlier results,[100] showing a frequency-dependent initial drop, a recurrence, and frequency-independent exponential decay at longer times (now with a time constant of about 2.5 ps,[171] due to the more realistic and slower SPC/E simulation model). Laage and Hynes[108,171] extended the separation-of-time-scale argument between spectral diffusion and rotation invoked earlier.[100] They first showed (from simulations of the SPC/E model) that the transition state for molecular rotation involves a bifurcated H-bond (described more fully below) and that the rate-limiting step for the rotation process involves the concerted arrival and departure of H-bond partners.[170] They then showed that the bifurcated transition state is extremely short-lived and will contribute negligibly to the absorption, even in the blue wing of the absorption band.[108] Therefore, exciting water molecules on the blue edge of the band does not specifically select molecules close to the transition state. However, the probability to evolve to the transition state within 125 fs is about five times larger in the blue wing of the absorption band than in the center.[171] This finding is consistent with the experimental observation of a dependence of the anisotropy decay on excitation frequency for delay times up to ~1 ps.[43] After spectral diffusion is complete (~1 ps), this frequency dependence will vanish, and the further decay of the ACF will be independent of pump and probe frequencies.

In the more recent studies in HDO:H_2O by Moilanen et al.[141] as described above, where the broad-band pump at $t = 0$ excites all molecules, the transient absorption probed at a time *t* later is frequency-resolved. These authors calculated $C_2(t)$ as done by Lawrence and Skinner,[100] averaging over only those molecules whose OH stretches are in (in this case very narrow) frequency windows at $t = 0$. Note that since trajectories from equilibrium simulations were used in this analysis and the classical equations of motion are fully time-reversible, this is equivalent to averaging over only those molecules whose OH stretches are in the same frequency windows at time *t*, which is consistent with the (broad-band pump/frequency-resolved probe) experiments.[141] Theoretical results[97] for a range of probe frequencies from the center of the band to the blue edge are shown in Figure 18, for the SPC/E simulation model and using a recently developed frequency map,[97,117] as described in section 2.2. One sees clearly the probe frequency dependence of the initial drop, followed by the recurrence described earlier. The values at 100 fs were reported in the paper by Moilanen et al.[141] and are also shown in Figure 15. Note that the recurrence time (and hence the librational frequency) is dependent on the probe frequency, ranging from about 56 fs at the center of the band to about 68 fs at the blue edge. These recurrence times correspond to librational frequencies of 595−490 cm^{-1}. Note that the former is in good agreement with the estimated librational frequency (585 cm^{-1}) of HDO:H_2O[141] and that the values of these librational frequencies and their trend with probe frequency are in qualitative agreement with those deduced from the harmonic cone model described above.[141]

The temperature dependences of the probe-frequency-dependent initial drops of C_2(100 fs) have also been calculated theoretically for HDO:H_2O,[97] and the results are

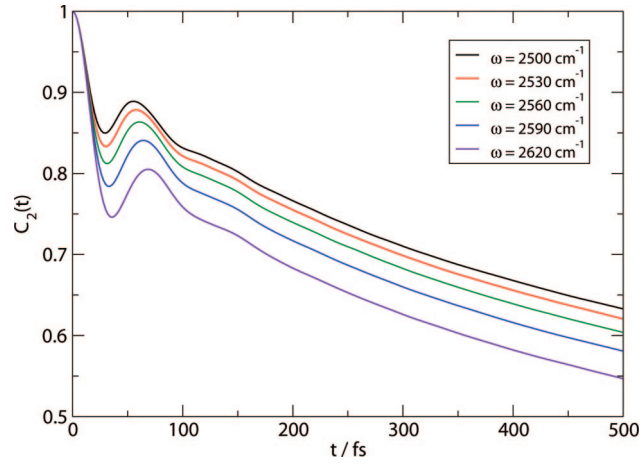

Figure 18. Calculated $C_2(t)$ for HDO:H_2O, as a function of probe frequency.[97] Reproduced with permission from ref 97. Copyright 2009 John Wiley and Sons.

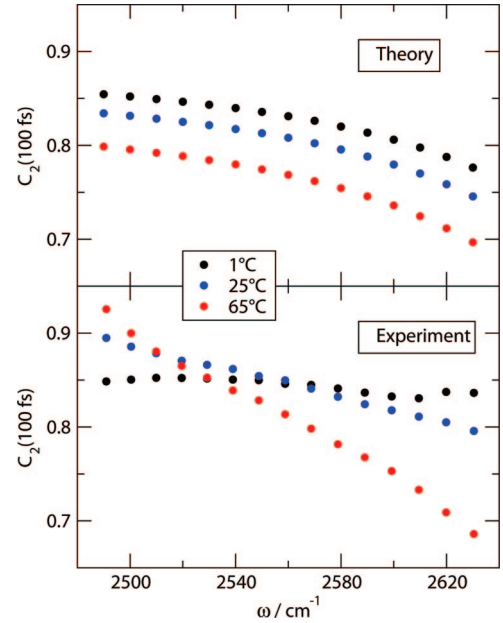

Figure 19. Experimental[141] and theoretical[97] initial drops of the rotational anisotropy correlation function, for HDO:H_2O, as a function of probe frequency, for three different temperatures. Reproduced with permission from ref 97. Copyright 2009 John Wiley and Sons.

compared with experiment[141] in Figure 19. In this case the theoretical results are in relatively poor agreement with experiment, showing neither the increased probe frequency dependence of the initial drop at higher temperature (65 °C) nor the nearly flat frequency dependence at 1 °C. Presumably this is due, at least in part, to the inability of the SPC/E model, which was parametrized at room temperature, to perform well at other temperatures. In particular, the freezing point of the SPC/E model is 215 K.[175] Moilanen et al. argue that the flat frequency dependence is a signature of collective dynamics very close to the freezing point, which would not be expected to be demonstrated by the SPC/E model at 1 °C (since this is so far above the freezing point for the model).

The last topic for this theoretical discussion involves the molecular mechanism of water rotation at long times, which, as discussed above at length, is characterized by a decay time of $C_2(t)$ for the OH bond unit vector of HDO:D_2O of about 3 ps and for the OD bond unit vector in HDO:H_2O of

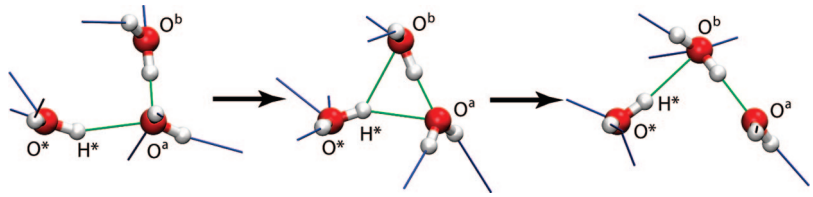

Figure 20. Schematic picture of the reorientation of water.[108] The rotating water molecule has oxygen and hydrogen atoms labeled with O* and H*, respectively. Reproduced with permission from ref 108. Copyright 2006 Elsevier.

about 2.5 ps. In two recent papers,[170,171] Laage and Hynes analyze trajectories from a simulation of SPC/E water, showing first of all that the picture based on small-step rotational diffusion is not correct. Rather, they find that rotations occur through large-amplitude angular jumps, involving a concerted H-bond switching event with a transition state characterized by a bifurcated H-bond. A schematic picture[108] of the molecular mechanism is shown in Figure 20. This picture is consistent with the interpretation of 2DIR spectra and associated calculations by Loparo et al.[158] As mentioned above, analysis of trajectories within the context of this extended jump model sheds further light on the frequency-dependent anisotropy decay at short times and its frequency independence at later times.[108] In addition, as described above, the 2DIR experiments of Tokmakoff and co-workers[151,158] and the two-color pump−probe anisotropy experiments of Bakker et al.[43] provide experimental support for this rotational mechanism.

5. Conclusions and Outlook

We have reviewed the contributions that vibrational spectroscopy in the OH/OD stretch regions of HDO:D_2O/HDO:H_2O has made to our understanding of the structure and dynamics of liquid water. We have focused on three classes of experimental observables: line shapes (IR and Raman), observables that probe spectral diffusion (hole-burning, integrated echoes, and 2DIR), and observables that probe molecular rotation (polarization-resolved pump−probe). In each case we have summarized the relevant experimental and theoretical studies.

Considering first the Raman line shapes, theoretical analysis indicates that the shoulder on the blue side is due to HOD molecules lacking an H-bond to the H/D atom for HDO:D_2O/HDO:H_2O, respectively.[114,117] Most of these broken H-bonded configurations are inherently unstable and, hence, are transient, and a small fraction of them correspond to bifurcated H-bond transition states.[151,158,171] In any case, most simulation models (together with an H-bond definition) indicate that 10−15% of the time a given H atom is not H-bonded. Thus, these broken H-bond configurations make an important contribution to the equilibrium structure of water. Theoretical analysis indicates that, in the H-bonding region of the line shapes, information about structure is not readily available, since, apparently, there is a poor correlation between OH/OD stretch frequency and H-bonding class.[117,126]

The spectral diffusion observables provide quite direct information about the frequency−frequency time-correlation function. Integrated three-pulse echo-peak shift experiments[140] show that the correlation function has an initial inertial time decay within 50 fs, a recurrence indicative of an underdamped oscillation at about 180 fs, and a long-time decay with a time constant of about 1.4 ps. Molecular dynamics simulations and other experiments support the idea that the underdamped oscillation is due to the intermolecular H-bond stretch. The initial decay on the 50 fs or shorter time scale is due to small-amplitude local rearrangements. The long-time decay time indicates the time scale over which the transition frequency becomes uncorrelated. Since the frequency is a functional of the nuclear positions of the surrounding molecules, this time scale is related to that for structural relaxation. Some have advanced the notion that this structural relaxation comes from making and breaking H-bonds with the HDO molecule,[99,100,103,104] while others have argued that the relaxation has a more long-range collective origin.[106] It is certainly possible that both are true;[104] for example, much of the relaxation on the 1 or 2 ps time scale may be due to making and breaking local hydrogen bonds, while the residual relaxation, possibly on slightly longer time scales, may be due to more collective processes. 2DIR experiments permit a more nuanced picture of spectral diffusion.[155,158] In particular, the finding that spectral diffusion is faster on the blue side is consistent with the intuitive idea that molecules with weak or broken H-bonds sample configuration space, and therefore frequency space, faster.

The pump−probe anisotropy experiments provide an equally intimate view of molecular rotation. The second-rank rotational time-correlation function also has an ultrafast decay within 100 fs, followed by a long-time exponential decay of 2.5−3 ps.[43,169,173] The former is found to depend on the frequencies of the pumping and probing light.[43,136,141] In general, on the blue side of the line the initial drop is largest, indicating more extensive orientational excursions. The amplitude of the drop can be related to the angle of an accessible cone or to the librational frequency of a harmonic cone potential. Pumping or probing on the blue side leads to larger cone angles or smaller cone librational frequencies. The subsequent exponential decay is frequency independent and characterizes the rotational relaxation time of the entire ensemble.[100,108] Since many rotational "attempts" are made before an actual rotational jump occurs, and during these attempts local, possibly including H-bond, rearrangements occur, which produce spectral diffusion, it is clear that the spectral diffusion time is faster than the rotational time. To rephrase this slightly differently, many configurational changes can cause spectral diffusion, but only a specific configuration involving the concerted departure and arrival of H-bond partners can lead to rotation. In this sense, spectral diffusion is a necessary but not sufficient condition for rotation.

Both sets of experiments lead to the following picture of motion in liquid water. Short-time dynamics is restricted, on the average, by both an angular potential and a translational potential, both due to H-bonding. For times less than 50 fs, a molecule can make small-amplitude angular and translational excursions near the bottom of this restraining potential, which lead to rapid but only partial loss of frequency and angular correlation. Theory and simulation predict that on slightly longer time scales these excursions lead to underdamped oscillations in both angular and

translational coordinates—the former is characterized by a librational frequency, and the latter is characterized by the hydrogen-bond stretch. Only the latter has been observed experimentally. At longer times molecules rotate and break hydrogen bonds, and as a result of recent 2DIR[155,158] and frequency-dependent pump−probe experiments[141,43] and simulations and theory,[100,106,108,141,170] the precise way in which this happens is now much clearer. Molecules rotate by way of a concerted H-bond switching event, going through a transition state with a weak bifurcated H-bond.[170] Thus, the molecule makes relatively infrequent but fast and large-amplitude angular jumps. The rate-limiting step is the approach of an H-bond accepting molecule. We anticipate that further frequency-dependent pump−probe experiments will undoubtedly refine the above picture of dynamics in liquid water.

Where do we go from here? Many of these same techniques can be, and in fact have already been, used to explore the structure and dynamics of water in other phases and in heterogeneous situations. For example, one can use vibrational spectroscopy to probe structure and dynamics in the many crystalline ice phases, in amorphous solid water, at the surfaces of solid and liquid water, and in the near-critical regime. One can use vibrational spectroscopy to probe the structure and dynamics of water in aqueous solutions of ionic and nonpolar species and in more heterogeneous situations such as in reverse micelles, in or near polymer or bilayer membranes, and in concentrated solutions of biomolecules. As in the case of liquid water, the exquisite sensitivity of OH stretch vibrational frequencies to local environments, coupled with the excellent time and frequency resolution of modern ultrafast vibrational spectroscopy, make this an excellent technique for unravelling complicated structural and dynamical issues in these fascinating and important systems.

6. Acknowledgments

The authors thank their research groups and collaborators for essential discussions about water over the past decade. H.J.B. thanks the Stichting Fundamenteel Onderzoek der Materie (Foundation for Fundamental Research on Matter) and the Nederlandse Organisatie voor Wetenschappelijk Onderzoek (Netherlands Organization for the Advancement of Research) for financial support. J.L.S. thanks Yu-Shan Lin for preparing several figures and for a critical reading of the manuscript and the National Science Foundation for support of this work through Grants CHE-0132538, CHE-0446666, and CHE-0750307.

7. References

(1) Ball, P. *Life's Matrix: A Biography of Water*; Farrar, Straus, and Giroux: New York, 1999.
(2) Ball, P. *Nature* **2008**, *452*, 291.
(3) Ball, P. *Chem. Rev.* **2008**, *108*, 74.
(4) Reed, A. E.; Weinhold, F.; Curtiss, L. A.; Pochatko, D. J. *J. Chem. Phys.* **1986**, *84*, 5687.
(5) Ojamäe, L.; Hermansson, K. *J. Phys. Chem.* **1994**, *98*, 4271.
(6) Pedulla, J. M.; Vila, F.; Jordan, K. D. *J. Chem. Phys.* **1996**, *105*, 11091.
(7) Xantheas, S. S. *Chem. Phys.* **2000**, *258*, 225.
(8) Kumar, R.; Skinner, J. L. *J. Phys. Chem. B* **2008**, *112*, 8311.
(9) Reed, A. E.; Curtiss, L. A.; Weinhold, F. *Chem. Rev.* **1988**, *88*, 899.
(10) Guillot, B. *J. Mol. Liq.* **2002**, *101*, 219.
(11) Car, R.; Parrinello, M. *Phys. Rev. Lett.* **1985**, *5*, 2471.
(12) Izvekov, S.; Voth, G. A. *J. Chem. Phys.* **2002**, *116*, 10372.
(13) Lee, H.-S.; Tuckerman, M. E. *J. Chem. Phys.* **2007**, *126*, 164501.
(14) Schwegler, E.; Grossman, J. C.; Gygi, F.; Galli, G. *J. Chem. Phys.* **2004**, *121*, 5400.
(15) Mantz, Y. A.; Chen, B.; Martyna, G. J. *J. Phys. Chem. B* **2006**, *110*, 3540.
(16) Todorova, T.; Seitsonen, A. P.; Hutter, J.; Kuo, I.-F. W.; Mundy, C. J. *J. Phys. Chem. B* **2006**, *110*, 3685.
(17) VandeVondele, J.; Mohamed, F.; Krack, M.; Hutter, J.; Sprik, M.; Parrinello, M. *J. Chem. Phys.* **2005**, *122*, 014515.
(18) Bukowski, R.; Szalewicz, K.; Groenenboom, G. C.; van der Avoird, A. *Science* **2007**, *315*, 1249.
(19) Fanourgakis, G. S.; Xantheas, S. S. *J. Phys. Chem. A* **2006**, *110*, 4100.
(20) Kuharski, R. A.; Rossky, P. J. *J. Chem. Phys.* **1985**, *82*, 5164.
(21) Poulsen, J. A.; Nyman, G.; Rossky, P. J. *J. Chem. Theory Comput.* **2006**, *2*, 1482.
(22) Stern, H. A.; Rittner, F.; Berne, B. J.; Friesner, R. A. *J. Chem. Phys.* **2001**, *115*, 2237.
(23) Paesani, F.; Iuchi, S.; Voth, G. A. *J. Chem. Phys.* **2007**, *127*, 074506.
(24) de la Peña, L. H.; Kusalik, P. G. *J. Chem. Phys.* **2004**, *121*, 5992.
(25) Paesani, F.; Voth, G. A. *J. Phys. Chem. B* **2009**, *113*, 5702.
(26) Ropp, J.; Lawrence, C.; Farrar, T. C.; Skinner, J. L. *J. Am. Chem. Soc.* **2001**, *123*, 8047.
(27) Smith, D. W. G.; Powles, J. G. *Mol. Phys.* **1966**, *10*, 451.
(28) Godralla, B. C.; Zeidler, M. D. *Mol. Phys.* **1986**, *59*, 817.
(29) Hardy, E. H.; Zygar, A.; Zeidler, M. D.; Holz, M.; Sacher, F. D. *J. Chem. Phys.* **2001**, *114*, 3174.
(30) Jonas, J.; DeFries, T.; Wilbur, D. J. *J. Chem. Phys.* **1976**, *65*, 582.
(31) Lang, E.; Lüdemann, H.-D. *J. Chem. Phys.* **1977**, *67*, 718.
(32) Barthel, J.; Bachhuber, K.; Buchner, R.; Hetzenauer, H. *Chem. Phys. Lett.* **1990**, *165*, 369.
(33) Head-Gordon, T.; Hura, G. *Chem. Rev.* **2002**, *102*, 2651.
(34) Wernet, P.; Nordlund, D.; Bergmann, U.; Cavalleri, M.; Odelius, M.; Ogasawara, H.; Näslund, L. Å.; Hirsch, T. K.; Ojamäe, L.; Glatzel, P.; Pettersson, L. G. M.; Nilsson, A. *Science* **2004**, *304*, 995.
(35) Smith, J. D.; Cappa, C. D.; Wilson, K. R.; Messer, B. M.; Cohen, R. C.; Saykally, R. J. *Science* **2004**, *306*, 851.
(36) Soper, A. K. *Chem. Phys.* **2000**, *258*, 121.
(37) Laage, D. *J. Phys. Chem. B* **2009**, *113*, 2684.
(38) Teixeira, J.; Bellissent-Funnel, M. C.; Chen, S. H.; Dianoux, A. J. *Phys. Rev. A* **1985**, *31*, 1913.
(39) Rønne, C.; Thrane, L.; Åstrand, P.-O.; Wallqvist, A.; Mikkelsen, K. V.; Keiding, S. R. *J. Chem. Phys.* **1997**, *107*, 5319.
(40) Rønne, C.; Åstrand, P.-O.; Keiding, S. R. *Phys. Rev. Lett.* **1999**, *82*, 2888.
(41) Prendergast, D.; Galli, G. *Phys. Rev. Lett.* **2006**, *96*, 215502.
(42) Nibbering, E. T. J.; Elsaesser, T. *Chem. Rev.* **2004**, *104*, 1887.
(43) Bakker, H. J.; Rezus, Y. L. A.; Timmer, R. L. A. *J. Phys. Chem. A* **2008**, *112*, 11523.
(44) Zheng, J.; Kwak, K.; Fayer, M. D. *Acc. Chem. Res.* **2007**, *40*, 75.
(45) Cho, M. *Chem. Rev.* **2008**, *108*, 1331.
(46) Auer, B.; Skinner, J. L. *J. Chem. Phys.* **2007**, *127*, 104105.
(47) Buch, V.; Tarbuck, T.; Richmond, G. L.; Groenzin, H.; Li, I.; Schultz, M. J. *J. Chem. Phys.* **2007**, *127*, 204710.
(48) Auer, B.; Skinner, J. L. *J. Chem. Phys.* **2008**, *128*, 224511.
(49) Woutersen, S.; Bakker, H. J. *Nature* **1999**, *402*, 507.
(50) Cowan, M. L.; Bruner, B. D.; Huse, N.; Dwyer, J. R.; Chugh, B.; Nibbering, E. T. J.; Elsaesser, T.; Miller, R. D. J. *Nature* **2005**, *434*, 199.
(51) Kraemer, D.; Cowan, M. L.; Paarmann, A.; Huse, N.; Nibbering, E. T. J.; Elsaesser, T.; Miller, R. J. D. *Proc. Natl. Acad. Sci. U.S.A.* **2008**, *105*, 437.
(52) Torii, H. *J. Phys. Chem. A* **2006**, *110*, 9469.
(53) Paarmann, A.; Hayashi, T.; Mukamel, S.; Miller, R. J. D. *J. Chem. Phys.* **2008**, *128*, 191103.
(54) Paarmann, A.; Hayashi, T.; Mukamel, S.; Miller, R. J. D. *J. Chem. Phys.* **2009**, *130*, 204110.
(55) Lock, A. J.; Bakker, H. J. *J. Chem. Phys.* **2002**, *117*, 1708.
(56) Pakoulev, A.; Wang, Z.; Dlott, D. D. *Chem. Phys. Lett.* **2003**, *371*, 594.
(57) Pakoulev, A.; Wang, Z.; Pang, Y.; Dlott, D. D. *Chem. Phys. Lett.* **2003**, *380*, 404.
(58) Wang, Z.; Pakoulev, A.; Pang, Y.; Dlott, D. D. *Chem. Phys. Lett.* **2003**, *378*, 281.
(59) Wang, Z.; Pakoulev, A.; Pang, Y.; Dlott, D. D. *J. Phys. Chem. A* **2004**, *108*, 9054.
(60) Wang, Z.; Pang, Y.; Dlott, D. D. *Chem. Phys. Lett.* **2004**, *397*, 40.
(61) Bakker, H. J.; Lock, A. J.; Madsen, D. *Chem. Phys. Lett.* **2004**, *384*, 236.
(62) Bakker, H. J.; Lock, A. J.; Madsen, D. *Chem. Phys. Lett.* **2004**, *385*, 329.
(63) Pakoulev, A.; Wang, Z.; Pang, Y.; Dlott, D. D. *Chem. Phys. Lett.* **2004**, *385*, 332.

(64) Huse, N.; Ashihara, S.; Nibbering, E. T. J.; Elsaesser, T. *Chem. Phys. Lett.* **2005**, *404*, 389.
(65) Lindner, J.; Vöhringer, P.; Pshenichnikov, M. S.; Cringus, D.; Wiersma, D. A.; Mostovoy, M. *Chem. Phys. Lett.* **2006**, *421*, 329.
(66) Ashihara, S.; Huse, N.; Espagne, A.; Nibbering, E. T. J.; Elsaesser, T. *Chem. Phys. Lett.* **2006**, *424*, 66.
(67) Ashihara, S.; Huse, N.; Espagne, A.; Nibbering, E. T. J.; Elsaesser, T. *J. Phys. Chem. A* **2007**, *111*, 743.
(68) Wang, Z.; Pang, Y.; Dlott, D. D. *J. Phys. Chem. A* **2007**, *111*, 3196.
(69) Roychowdhury, S.; Bagchi, B. *Chem. Phys.* **2008**, *343*, 76.
(70) Mallik, B. S.; Semparithi, A.; Chandra, A. *J. Phys. Chem. A* **2008**, *112*, 5104.
(71) Ingrosso, F.; Rey, R.; Elsaesser, T.; Hynes, J. T. *J. Phys. Chem. A* **2009**, *113*, 6657.
(72) Nicodemus, R. A.; Tokmakoff, A. *Chem. Phys. Lett.* **2007**, *449*, 130.
(73) Rey, R.; Møller, K. B.; Hynes, J. T. *Chem. Rev.* **2004**, *104*, 1915.
(74) Woutersen, S.; Emmerichs, U.; Nienhuys, H.-K.; Bakker, H. J. *Phys. Rev. Lett.* **1998**, *81*, 1106.
(75) Gale, G. M.; Gallot, G.; Lascoux, N. *Chem. Phys. Lett.* **1999**, *311*, 123.
(76) Deàk, J. C.; Rhea, S. T.; Iwaki, L. K.; Dlott, D. D. *J. Phys. Chem. A* **2000**, *104*, 4866.
(77) Schwarzer, D.; Lindner, J.; Vöhringer, P. *J. Chem. Phys.* **2005**, *123*, 161105.
(78) Rey, R.; Hynes, J. T. *J. Chem. Phys.* **1996**, *104* (6), 2356.
(79) Lawrence, C. P.; Skinner, J. L. *J. Chem. Phys.* **2002**, *117*, 5827.
(80) Lawrence, C. P.; Skinner, J. L. *J. Chem. Phys.* **2003**, *119*, 1623.
(81) Lawrence, C. P.; Skinner, J. L. *J. Chem. Phys.* **2003**, *119*, 3840.
(82) Kropman, M. F.; Nienhuys, H.-K.; Woutersen, S.; Bakker, H. J. *J. Phys. Chem. A* **2001**, *105*, 4622.
(83) Larsen, O. F. A.; Woutersen, S. *J. Chem. Phys.* **2004**, *121*, 12143.
(84) Bodis, P.; Larsen, O. F. A.; Woutersen, S. *J. Phys. Chem. A* **2005**, *109*, 5303.
(85) Brubach, J. B.; Mermet, A.; Filabozzi, A.; Gerschel, A.; Roy, R. *J. Chem. Phys.* **2005**, *122*, 184509.
(86) Schmidt, D. A.; Miki, K. *J. Phys. Chem. A* **2007**, *111*, 10119.
(87) Graener, H.; Seifert, G.; Laubereau, A. *Phys. Rev. Lett.* **1991**, *66*, 2092.
(88) Laenen, R.; Rauscher, C.; Laubereau, A. *Phys. Rev. Lett.* **1998**, *80*, 2622.
(89) Laenen, R.; Rauscher, C.; Laubereau, A. *J. Phys. Chem. B* **1998**, *102*, 9304.
(90) Laenen, R.; Simeonidis, K.; Laubereau, A. *J. Phys. Chem. B* **2002**, *106*, 408.
(91) Gordon, R. G. *Adv. Magn. Reson.* **1968**, *3*, 1.
(92) Skinner, J. L. *Mol. Phys.* **2008**, *106*, 2245.
(93) Ahlborn, H.; Ji, X.; Space, B.; Moore, P. B. *J. Chem. Phys.* **1999**, *111*, 10622.
(94) Martí, J.; Guàrdia, E.; Padró, J. A. *J. Chem. Phys.* **1994**, *101*, 1083.
(95) Mankoo, P. K.; Keyes, T. *J. Chem. Phys.* **2008**, *129*, 034504.
(96) Silvestrelli, P. L.; Bernasconi, M.; Parrinello, M. *Chem. Phys. Lett.* **1997**, *277*, 478.
(97) Skinner, J. L.; Auer, B. M.; Lin, Y.-S. *Adv. Chem. Phys.* **2009**, *142*, 59.
(98) Lawrence, C. P.; Skinner, J. L. *J. Chem. Phys.* **2002**, *117*, 8847.
(99) Lawrence, C. P.; Skinner, J. L. *Chem. Phys. Lett.* **2003**, *369*, 472.
(100) Lawrence, C. P.; Skinner, J. L. *J. Chem. Phys.* **2003**, *118*, 264.
(101) Piryatinski, A.; Lawrence, C. P.; Skinner, J. L. *J. Chem. Phys.* **2003**, *118*, 9664.
(102) Piryatinski, A.; Lawrence, C. P.; Skinner, J. L. *J. Chem. Phys.* **2003**, *118*, 9672.
(103) Rey, R.; Møller, K. B.; Hynes, J. T. *J. Phys. Chem. A* **2002**, *106*, 11993.
(104) Møller, K. B.; Rey, R.; Hynes, J. T. *J. Phys. Chem. A* **2004**, *108*, 1275.
(105) Fecko, C. J.; Eaves, J. D.; Loparo, J. J.; Tokmakoff, A.; Geissler, P. L. *Science* **2003**, *301*, 1698.
(106) Eaves, J. D.; Tokmakoff, A.; Geissler, P. L. *J. Phys. Chem. A* **2005**, *109*, 9424.
(107) Harder, E.; Eaves, J. D.; Tokmakoff, A.; Berne, B. J. *Proc. Natl. Acad. Sci. U.S.A.* **2005**, *102*, 11611.
(108) Laage, D.; Hynes, J. T. *Chem. Phys. Lett.* **2006**, *433*, 80.
(109) Diraison, M.; Guissani, Y.; Leicknam, J.-C.; Bratos, S. *Chem. Phys. Lett.* **1996**, *258*, 348.
(110) Hermansson, K.; Knuts, S.; Lindgren, J. *J. Chem. Phys.* **1991**, *95*, 7486.
(111) Hayashi, T.; l. C. Jansen, T.; Zhuang, W.; Mukamel, S. *J. Phys. Chem. A* **2005**, *109*, 64.
(112) Corcelli, S. A.; Lawrence, C. P.; Skinner, J. L. *J. Chem. Phys.* **2004**, *120*, 8107.
(113) Berendsen, H. J. C.; Grigera, J. R.; Straatsma, T. P. *J. Phys. Chem.* **1987**, *91*, 6269.
(114) Corcelli, S. A.; Skinner, J. L. *J. Phys. Chem. A* **2005**, *109*, 6154.
(115) Schmidt, J. R.; Corcelli, S. A.; Skinner, J. L. *J. Chem. Phys.* **2005**, *123*, 044513.
(116) Schmidt, J. R.; Roberts, S. T.; Loparo, J. J.; Tokmakoff, A.; Fayer, M. D.; Skinner, J. L. *Chem. Phys.* **2007**, *341*, 143.
(117) Auer, B.; Kumar, R.; Schmidt, J. R.; Skinner, J. L. *Proc. Natl. Acad. Sci. U.S.A.* **2007**, *104*, 14215.
(118) Auer, B.; Skinner, J. L. *J. Chem. Phys.* **2008**, *129*, 214705.
(119) Whalley, E.; Klug, D. D. *J. Chem. Phys.* **1986**, *84*, 78.
(120) Hadži, D.; Bratos, S. In *The Hydrogen Bond*; Schuster, P., Zundel, G., Sandorfy, C., Eds.; Elsevier: Amsterdam, 1976; Vol. 2, Chapter 12.
(121) Pimentel, G. C.; McClellan, A. L. *The Hydrogen Bond*; W. H. Freeman and Company: San Francisco, 1960.
(122) Mukamel, S. *Principles of Nonlinear Optical Spectroscopy*; Oxford: New York, 1995.
(123) Kubo, R. *Adv. Chem. Phys.* **1969**, *15*, 101.
(124) Smith, J. D.; Cappa, C. D.; Wilson, K. R.; Cohen, R. C.; Geissler, P. L.; Saykally, R. J. *Proc. Natl. Acad. Sci. U.S.A.* **2005**, *102*, 14171.
(125) Lin, Y.-S.; Auer, B. M.; Skinner, J. L. *J. Chem. Phys.* **2009**, *131*, 144511.
(126) Auer, B.; Skinner, J. L. *Chem. Phys. Lett.* **2009**, *470*, 13.
(127) Loparo, J. J.; Roberts, S. T.; Nicodemus, R. A.; Tokmakoff, A. *Chem. Phys.* **2007**, *341*, 218.
(128) Kumar, R.; Schmidt, J. R.; Skinner, J. L. *J. Chem. Phys.* **2007**, *126*, 204107.
(129) Eisenberg, D.; Kauzmann, W. *The Structure and Properties of Water*; Oxford University Press: New York, 1969.
(130) Jimenez, R.; Fleming, G. R.; Kumar, P. V.; Maroncelli, M. *Nature* **1994**, *369*, 471.
(131) Ohmine, I.; Saito, S. *Acc. Chem. Res.* **1999**, *32*, 741.
(132) Mikenda, W. *J. Mol. Struct.* **1986**, *147*, 1.
(133) Steinel, T.; Asbury, J. B.; Zheng, J.; Fayer, M. D. *J. Phys. Chem. A* **2004**, *108*, 10958.
(134) Woutersen, S.; Emmerichs, U.; Bakker, H. J. *Science* **1997**, *278*, 658.
(135) Nienhuis, H.-K.; van Santen, R. A.; Bakker, H. J. *J. Chem. Phys.* **2000**, *112*, 8487.
(136) Bakker, H. J.; Woutersen, S.; Nienhuys, H.-K. *Chem. Phys.* **2000**, *258*, 233.
(137) Gallot, G.; Bratos, S.; Pommeret, S.; Lascoux, N.; Leicknam, J.-C.; Koziński, M.; Amir, W.; Gale, G. M. *J. Chem. Phys.* **2002**, *117*, 11301.
(138) Rezus, Y. L. A.; Bakker, H. J. *J. Chem. Phys.* **2006**, *125*, 144512.
(139) Rezus, Y. L. A.; Bakker, H. J. *J. Chem. Phys.* **2005**, *123*, 114502.
(140) Fecko, C. J.; Loparo, J. J.; Roberts, S. T.; Tokmakoff, A. *J. Chem. Phys.* **2005**, *122*, 054506.
(141) Moilanen, D. E.; Fenn, E. E.; Lin, Y.-S.; Skinner, J. L.; Bagchi, B.; Fayer, M. D. *Proc. Natl. Acad. Sci. U.S.A.* **2008**, *105*, 5295.
(142) Gale, G. M.; Gallot, G.; Hache, F.; Lascoux, N.; Bratos, S.; Leicknam, J.-C. *Phys. Rev. Lett.* **1999**, *82*, 1068.
(143) Woutersen, S.; Bakker, H. J. *Phys. Rev. Lett.* **1999**, *83*, 2077.
(144) Bakker, H. J.; Nienhuys, H.-K.; Gallot, G.; Lascoux, N.; Gale, G. M.; Leicknam, J.-C.; Bratos, S. *J. Chem. Phys.* **2002**, *116*, 2592.
(145) Cho, M.; Yu, J.-Y.; Joo, T.; Nagasawa, Y.; Passino, S. A.; Fleming, G. R. *J. Phys. Chem.* **1996**, *100*, 11944.
(146) Piryatinski, A.; Skinner, J. L. *J. Phys. Chem. B* **2002**, *106*, 8055.
(147) Stenger, J.; Madsen, D.; Hamm, P.; Nibbering, E. T. J.; Elsaesser, T. *J. Phys. Chem. A* **2002**, *106*, 2341.
(148) Yeremenko, S.; Pshenichnikov, M. S.; Wiersma, D. A. *Phys. Rev. A* **2006**, *73*, 021804.
(149) Stenger, J.; Madsen, D.; Hamm, P.; Nibbering, E. T. J.; Elsaesser, T. *Phys. Rev. Lett.* **2001**, *87*, 027401.
(150) Yeremenko, S.; Pshenichnikov, M. S.; Wiersma, D. A. *Chem. Phys. Lett.* **2003**, *369*, 107.
(151) Eaves, J. D.; Loparo, J. J.; Fecko, C. J.; Roberts, S. T.; Tokmakoff, A.; Geissler, P. L. *Proc. Natl. Acad. Sci. U.S.A.* **2005**, *102*, 13019.
(152) Asbury, J. B.; Steinel, T.; Stromberg, C.; Corcelli, S. A.; Lawrence, C. P.; Skinner, J. L.; Fayer, M. D. *J. Phys. Chem. A* **2004**, *108*, 1107.
(153) Roberts, S. T.; Loparo, J. J.; Tokmakoff, A. *J. Chem. Phys.* **2006**, *125*, 084502.
(154) Kwak, K.; Park, S.; Finkelstein, I. J.; Fayer, M. D. *J. Chem. Phys.* **2007**, *127*, 124503.
(155) Steinel, T.; Asbury, J. B.; Corcelli, S. A.; Lawrence, C. P.; Skinner, J. L.; Fayer, M. D. *Chem. Phys. Lett.* **2004**, *386*, 295.
(156) Asbury, J. B.; Steinel, T.; Kwak, K.; Corcelli, S. A.; Lawrence, C. P.; Skinner, J. L.; Fayer, M. D. *J. Chem. Phys.* **2004**, *121*, 12431.
(157) Loparo, J. J.; Roberts, S. T.; Tokmakoff, A. *J. Chem. Phys.* **2006**, *125*, 194521.
(158) Loparo, J. J.; Roberts, S. T.; Tokmakoff, A. *J. Chem. Phys.* **2006**, *125*, 194522.
(159) l. C. Jansen, T.; Hayashi, T.; Zhuang, W.; Mukamel, S. *J. Chem. Phys.* **2005**, *123*, 114504.
(160) Corcelli, S. A.; Lawrence, C. P.; Asbury, J. B.; Steinel, T.; Fayer, M. D.; Skinner, J. L. *J. Chem. Phys.* **2004**, *121*, 8897.

(161) Rick, S. W.; Stuart, S. J.; Berne, B. J. *J. Chem. Phys.* **1994**, *101*, 6141.
(162) Garrett-Roe, S.; Hamm, P. *J. Chem. Phys.* **2008**, *128*, 104507.
(163) Winkler, K.; Lindner, J.; Bürsing, H.; Vöhringer, P. *J. Chem. Phys.* **2000**, *113*, 4674.
(164) Lankhorst, D.; Schriever, J.; Leyte, J. C. *Ber. Bunsen-Ges. Phys.Chem.* **1982**, *86*, 215.
(165) van der Maarel, J. R. C.; Lankhorst, D.; de Bleijser, J.; Leyte, J. C. *Chem. Phys. Lett.* **1985**, *122*, 541.
(166) Lipari, G.; Szabo, A. *Biophys. J.* **1980**, *30*, 489.
(167) Kandratsenka, A.; Schroeder, J.; Schwarzer, D.; Vikhrenko, V. S. *J. Chem. Phys.* **2009**, *130*, 174507.
(168) Timmer, R. L. A.; Bakker, H. J. *J. Chem. Phys.* **2007**, *126*, 154507.
(169) Piletic, I. R.; Moilanen, D. E.; Spry, D. B.; Levinger, N. E.; Fayer, M. D. *J. Phys. Chem. A* **2006**, *110*, 4985.
(170) Laage, D.; Hynes, J. T. *Science* **2006**, *311*, 832.
(171) Laage, D.; Hynes, J. T. *J. Phys. Chem. B* **2008**, *112*, 14230.
(172) Wallqvist, A.; Berne, B. J. *J. Phys. Chem.* **1993**, *97*, 13841.
(173) Loparo, J. J.; Fecko, C. J.; Eaves, J. D.; Roberts, S. T.; Tokmakoff, A. *Phys. Rev. B* **2004**, *70*, 180201.
(174) Jorgensen, W. L.; Chandrasekhar, J.; Madura, J. D.; Impey, R. W.; Klein, M. L. *J. Chem. Phys.* **1983**, *79*, 926.
(175) Vega, C.; Sanz, E.; Abascal, J. L. F. *J. Chem. Phys.* **2005**, *122*, 114507.

CR9001879